Journal of Medicinal Chemistry

Article

Discovery of LOU064 (Remibrutinib), a Potent and Highly Selective Covalent Inhibitor of Bruton's Tyrosine Kinase

Daniela Angst, François Gessier, Philipp Janser, Anna Vulpetti, Rudolf Wälchli, Christian Beerli, Amanda Littlewood-Evans, Janet Dawson, Barbara Nuesslein-Hildesheim, Grazyna Wieczorek, Sascha Gutmann, Clemens Scheufler, Alexandra Hinniger, Alfred Gilbert Zimmerlin, Enrico G. Funhoff, Robert Pulz, and Bruno Cenni

J. Med. Chem., **Just Accepted Manuscript** • DOI: 10.1021/acs.jmedchem.9b01916 • Publication Date (Web): 21 Feb 2020

Just Accepted

is published by the American Chemical Society. 1155 Sixteenth Street N.W., Washington, DC 20036

Discovery of LOU064 (Remibrutinib), a Potent and Highly Selective Covalent Inhibitor of Bruton's Tyrosine Kinase

Daniela Angst[a], François Gessier[a], Philipp Janser[a], Anna Vulpetti[a], Rudolf Wälchli[a], Christian Beerli[b], Amanda Littlewood-Evans[b], Janet Dawson[b], Barbara Nuesslein-Hildesheim[b], Grazyna Wieczorek[b], Sascha Gutmann[c], Clemens Scheufler[c], Alexandra Hinniger[c], Alfred Zimmerlin[d], Enrico G. Funhoff[e], Robert Pulz[a], Bruno Cenni[b]*

[a]Global Discovery Chemistry, [b]Autoimmunity, Transplantation & Inflammation, [c]Chemical Biology & Therapeutics, [d]PK Sciences, [e]Preclinical Safety, Novartis Institutes for BioMedical Research, Novartis Campus, CH-4002 Basel, Switzerland

Abstract. Bruton's tyrosine kinase (BTK), a cytoplasmic tyrosine kinase, plays a central role in immunity and is considered an attractive target for treating autoimmune diseases. The use of currently marketed covalent BTK inhibitors is limited to oncology indications based on their suboptimal kinase selectivity. We describe the discovery and preclinical profile of LOU064 (remibrutinib, **25**), a potent, highly selective covalent BTK inhibitor. LOU064 exhibits an exquisite kinase selectivity due to binding to an inactive conformation of BTK and has the potential for a best-in-class covalent BTK inhibitor for the treatment of autoimmune diseases. It

demonstrates potent *in vivo* target occupancy with an EC_{90} of 1.6 mg/kg and dose-dependent efficacy in rat collagen-induced arthritis. LOU064 is currently being tested in Phase 2 clinical studies for chronic spontaneous urticaria and Sjoegren's Syndrome.

INTRODUCTION

Bruton's tyrosine kinase (BTK) is a cytoplasmic tyrosine kinase selectively expressed in a subset of immune cells, including macrophages, mast cells, basophils, platelets and B cells, but not in mature plasma cells and T cells.[1,2] BTK is activated by membrane recruitment via its pleckstrin homology domain and phosphorylation of the activation loop Tyr551 by SYK and SRC family kinases, resulting in autophosphorylation of Tyr223 in the SH3 domain.[1,2] BTK is an essential node and rheostat for the signaling of the antigen receptor in B cells (BCR) and of activating Fc receptors for IgG and IgE (FcγR, FcεR) in macrophages and mast cells.[3–5] While inborn BTK deficiency does not affect the development of many immune cells, it results in severely impaired B cell development and antibody production.[6–8] In humans BTK deficiency is the most frequent cause of the primary immunodeficiency X-linked agammaglobulinemia (XLA), a condition that if untreated is associated with an increased bacterial infection risk.[9] Today XLA is treated by immunoglobulin replacement therapy suggesting that the main risk factor for infections is the absence of protective immunoglobulins rather than the deficiency in cellular BTK function.[10] The role of BTK appears not to be critical for B cell survival once the B cells have developed, suggesting that BTK inhibition after infancy may not lead to acute B cell and antibody depletion.[6]

The potential role of BTK in autoimmunity, allergy and chronic inflammatory conditions is supported by genetic validation in many rodent models for arthritis, systemic lupus erythematosus and anaphylaxis.[3,11–13] More recently, the functional relevance of BTK has also been validated by pharmacological inhibition in various clinical trials and is testament for the activities across many pharmaceutical companies to identify and develop BTK inhibitors, both covalent and reversible.[14–22]

The kinase domain of BTK contains Cys481 in a position conserved in a group of eleven kinases including the closely related TEC family kinases BMX, TEC, ITK and TXK, as well as in EGFR, ERBB2, ERBB4, JAK3, BLK and MKK7.[23,24] These conserved cysteines have been targeted in the development of covalent inhibitors of BTK, EGFR, JAK3 and MKK7. The concept of selective targeted covalent kinase inhibitors has received more attention due its potential for sustained target inhibition, uncoupled from sustained and high systemic drug exposure. This special pharmacologic feature of covalent inhibitors may lead to high efficacy and an improved safety profile.[25,26]

The covalent BTK inhibitors ibrutinib (**1**) and acalabrutinib (**2**) (Figure 1, a)) have shown efficacy and an attractive risk-benefit profile leading to their approval in several B cell malignancies including chronic lymphocytic leukemia and mantle cell lymphoma.[27] Due to its binding to BTK in its active conformation, ibrutinib (**1**) not only potently inhibits BTK, but irreversibly inhibits all kinases which carry a Cys at the same position as BTK, and in addition inhibits reversibly several other kinases.[14,28,29] While the clinical efficacy of **1** is of significant benefit in difficult to treat oncologic indications, its side effect profile precludes its use in rheumatologic indications.[30–34] It is likely that its off-target activity is associated with the clinical risk for skin rash and diarrhea (well established for EGFR inhibitors[35]), or platelet disfunction

(shown for TEC and SRC kinases[36,37]). Second generation clinical-stage covalent inhibitors such as acalabrutinib (**2**), tirabrutinib (**3**), evobrutinib (**4**) and branebrutinib (**5**) (Figure 1, a)) retain a similar binding mode to BTK as **1** and therefore, despite offering an overall improved kinase selectivity profile, still inhibit several Cys-containing kinases.[18,22,38–40]

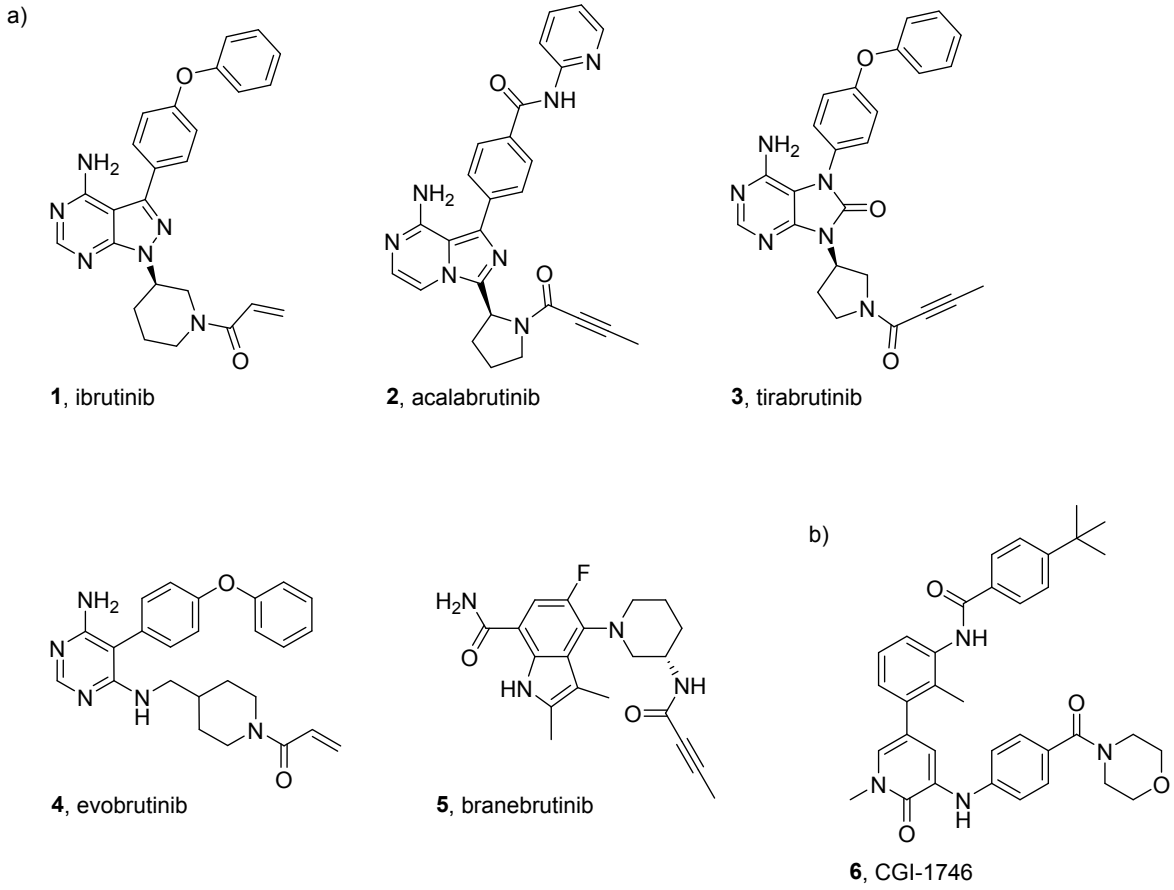

Figure 1. a) Selected examples of covalent BTK inhibitors (**1**-**5**); b) Structure of CGI-1746 (**6**), the first reported compound binding to an inactive BTK conformation.

Reversible BTK inhibitors with high kinase selectivity have been described[15,16,21,41] and CGI-1746 (**6**) (Figure 1, b)) was the first compound reported to bind to an inactive conformation

of BTK resulting in an excellent kinase selectivity. This binding mode prevents the phosphorylation of Tyr551in the activation loop of BTK by upstream kinases and possibly contributes to higher cellular potency.[42] In contrast to covalent inhibitors, reversible inhibitors require continuous systemic drug exposure over the entire dosing interval in order to maintain a high degree of target inhibition. In order to achieve this, intensive efforts were necessary to optimize the profile of **6**, including ADME properties, potency, and safety, while maintaining the specific binding mode, finally leading to GDC-0853 (fenebrutinib), a selective reversible BTK inhibitor currently in Phase 2 clinical trials.[21]

We were attracted by the concept of covalent BTK inhibition as it allows the optimization of compounds for a potent and sustained pharmacodynamic effect without the need for extended and high systemic compound exposure.[25] At the same time, we wanted to differentiate from competitor molecules by aiming for a very high selectivity to minimize kinase off-target reversible and covalent binding. Therefore we selected the strategy of combining the advantages of the covalent MoA with targeting the inactive conformation of BTK.

RESULTS AND DISCUSSION

The concept of combining a reversible BTK inhibitor binding to an inactive conformation of BTK with a warhead leading to highly selective, covalent BTK inhibitors has been recently published by us and others. [43,44] We disclosed the discovery of a series of pyrrolopyrimidines. Using compound **7** (BTK enzyme IC_{50} of 0.013 ± 0.0078 μM, Figure 2) as starting point, a reversible BTK inhibitor binding to the same inactive BTK conformation as **6**, we designed inhibitors forming a covalent bond with Cys481. The compounds of this series, represented by **8**

(BTK enzyme IC_{50} of 0.0009 ± 0.0005 μM, Figure 2), are potent inhibitors of BTK *in vitro* and we were able to demonstrate BTK occupancy after oral dosing in a PK/PD model. However, the pyrrolopyrimidine series suffered from very high *in vivo* clearance, making it challenging to achieve *in vivo* efficacy at low doses. Thorough investigation of the pyrrolopyrimidine SAR did not lead to a significantly improved PK profile. Therefore, we decided to explore alternative hinge binders with the aim of improving the ADME properties, while keeping the key interactions with BTK, as displayed in the X-ray cocrystal structure of **7** (Figure 3). Replacing the pyrrolopyrimidine moiety by 6-aminopyrimidine as hinge binder motif provided **9** (Figure 2) as a reversible prototype. Figure 3 shows the model of the aminopyrimidine **9** bound to the inactive conformation of BTK based on the solved crystal structure with **7**. In the model, the aminopyrimidine scaffold forms the same key interactions with BTK as the pyrrolopyrimidine **7** with the exception of the contacts at the entrance of the ATP binding pocket. The removed phenyl at position **6** of compound **7** is nicely sandwiched between the side chains of Leu408 and Gly480. For that reason, some loss of affinity was expected.

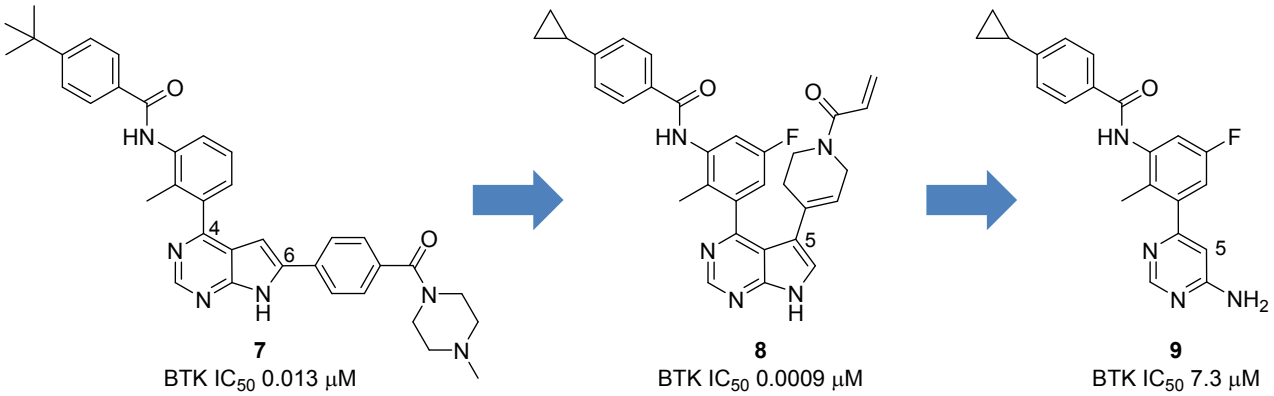

Figure 2. Morphing of the pyrrolopyrimidine scaffold to an aminopyrimidine scaffold. BTK enzyme inhibition in Caliper assay, IC_{50} shown.

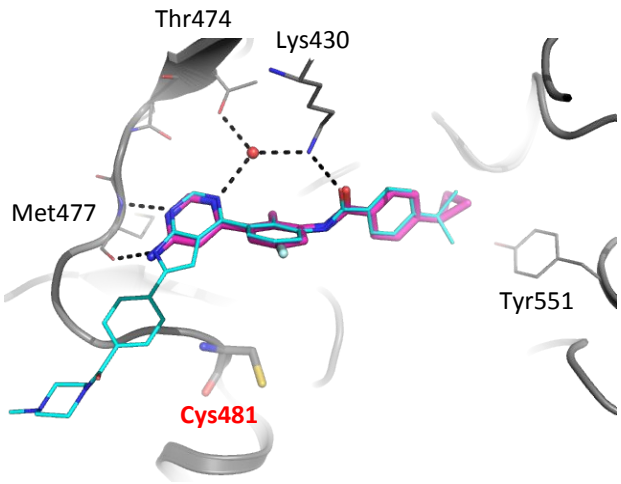

Figure 3. Crystal structure of **7** (PDB 6S90; in cyan) in complex with human BTK overlaid with the binding model of compound **9**. H-bonds of the pyrrolopyrimidine and 6-aminopyrimidine scaffold (in purple) to Met477 and a water molecule (red sphere) are highlighted (black dashed lines), as well as the hydrogen bond between the carbonyl of the amide of the ligand and Lys430 side chain.

Indeed, compound **9** inhibited BTK in an enzymatic assay with an IC_{50} of 7.3 ± 0.35 μM, confirming our morphing idea. Similarily to what we described for the pyrrolopyrimidine scaffold,[43] we envisaged to generate potent and selective covalent inhibitors by introducing a linker with a warhead at position 5 of the pyrimidine moiety to reach Cys481. We started with acrylamide warheads, as they have been used successfully in covalent BTK inhibitors such as **1** and **4**.[45]

SAR: Optimizing *in vivo* BTK Occupancy. We first investigated alkene based linkers between the pyrimidine core and the warhead providing a somewhat rigidified exit vector. Introducing a three carbon linker (**10**) and a four carbon linker (**11**) led to moderately potent

compounds in the BCR/CD69 assay in blood (Table 1). However, **10** and **11** suffered from very high clearance in rat liver microsomes (CL_{int} 924 and 815 μL/min/mg, respectively). Replacing the carbon linkers with 3-oxypyrrolidine (**12**) was not tolerated with respect to BTK inhibition, but the metabolic stability significantly increased (CL_{int} 135 μL/min/mg). Switching to a 3-oxyazetidine linker (**13**) led to an improvement of blood BCR/CD69 potency and good metabolic stability (CL_{int} 25 μL/min/mg). Having succesfully combined these two properties, we sought to assess the *in vivo* PD effect of **13** by measuring BTK occupancy in rat spleen after a single oral dose (Experimental Section). Administration of **13** (10 mg/kg po) provided 36 % BTK occupancy and blood levels of 13 nM 5 h post dose. A rat PK of **13** revealed a bioavailability of only 5 %, likely limited by the low permeability. Therefore we set out to optimize the permeability, since improved oral absorption should subsequently increase target occupancy. We envisioned that introducing a fluoro substituent ortho to the amide on the phenyl ring occupying the H3 pocket could form an internal hydrogen bond in solution, masking the amide NH and leading to improved permeability.[46] The fluoro substituent was tolerated with respect to potency and **14** indeed displayed improved permeability by more than one log unit compared to **13**. This led to a higher bioavailability of 51 % in a rat PK study and resulted in 96 % target occupancy after a 10 mg/kg po dose. Lowering the dose of **14** to 3 mg/kg po and 1 mg/kg po still provided BTK occupancy of 79 % and 44 %, respectively. In an effort to further improve the potency we investigated two alternative moieties in the H3 pocket, which in previous studies on a related reversible series (not shown) had provided a positive effect on the potency. Surprisingly, replacing the cyclopropyl substituent in **14** with 2-hydroxypropanyl (**15**) led to a decreased potency in the blood BCR/CD69 assay. Introducing a second fluoro substituent (**16**) recovered the blood potency, however the permeability of **16** was poor,

translating into a modest target occupancy of only 32 % after a dose of 3 mg/kg po. Based on the promising results of **14** in the BTK occupancy assay, we profiled the compound more broadly. However, the stability of **14** in human plasma turned out to be low ($t_{1/2}$ 35 min). Plasma instability could be an indication of an undesired covalent binding to plasma proteins or enzymatic cleavage, therefore we used this assay to optimize our scaffold.

Table 1. Linker and tail modifications.

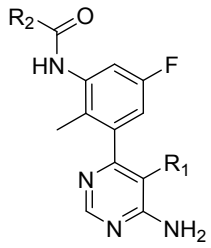

	R_1	R_2	BTK IC_{50} [nM][a]	FcγR/IL8 IC_{50} [nM][b]	BCR/CD69 IC_{50} [nM][c]	Permeability logPe pH 6.8[d]	BTK occupancy [%] (Dose [mg/kg])[e]
10	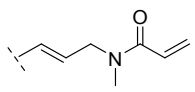	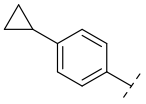	3.8 ± 0.32	11 ± 6	106 ± 51	-5.0	n.t.
11	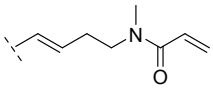	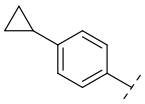	1.8[e]	15 ± 4	223 ± 18	-4.6	n.t.
12	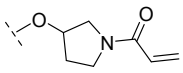	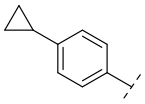	3651 ± 3619	1437 ± 309	n.t.	-6.2	n.t.
13	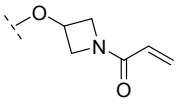	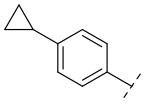	3.6 ± 0.66	17 ± 3	95 ± 4	<-6.7	36 (10)
14	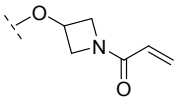	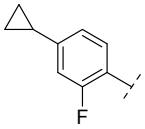	4.5 ± 1.6	20 ± 13	86 ± 30	-5.2	96 (10) 79 (3) 44 (1)
15	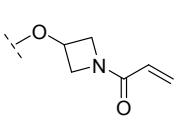	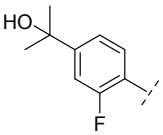	23 ± 10	108 ± 78	250 ± 0	-6.6	n.t.
16	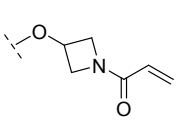	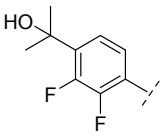	2.3 ± 1.1	24 ± 7	55 ± 29	<-6.6	32 (3)

a) BTK enzyme inhibition in Caliper assay IC_{50} shown as means ± SD ($n \geq 2$); b) FcγR induced IL8 IC_{50} shown as means ± SD ($n \geq 2$); c) anti-IgM/IL-4 induced CD69 expression on human blood B cells IC_{50} shown as means ± SD ($n \geq 2$); d) PAMPA permeability, logPe at pH 6.8; e) BTK occupancy in rat spleen homogenate 5 h after po dose of compounds compared to vehicle control, determined as mean ($n = 3$); e) $n = 1$; f) n.t.: not tested.

We sought to investigate the linker to the warhead more broadly with the goal to increase the plasma stability and in addition to further improve blood potency and *in vivo* PD. We combined various linkers with the most attractive H3 pocket moiety, the fluorinated cyclopropylphenyl tail. The propenyl linker (**17**) led to a two fold increase in potency in the blood BCR/CD69 assay compared to **14** and good plasma stability (Table 2). However, the increased blood potency did not translate into an improved PD effect, **17** performed similarly to **14** *in vivo*, providing 77 % BTK occupancy, probably due to the high *in vivo* clearance (307 ml/min/kg). The oxygen linked open-chain analogue **18** was in the same potency range as **14**, and gave high target occupancy of 84 % despite its only moderate permeability. Replacing the linker oxygen by a nitrogen (**19**) was not tolerated leading to a roughly 10-fold loss of potency in the human blood assay. Despite a more than two-fold reduced blood potency compared to **14**, introduction of a piperidine linker gave similar target occupancy, due to high exposure (207 nM 5 h post dose). Whereas the (R)-pyrrolidine linker (**21**) was not tolerated with respect to BTK inhibition, the (S)-derivative **22** potently inhibited the blood BCR/CD69 assay and BTK occupancy of 90 % was achieved. However, **22** suffered from a strong hERG flag (hERG dofetilide binding IC_{50} 49 ± 12 nM (n = 2)). Replacing the pyrrolidine moiety by an azetidine provided **23**, which achieved 80 % BTK occupancy. However, as in the case of azetidine **14**, plasma stability of **23** was low. An enhanced reactivity of N-acryloyl azetidines towards cysteines has been reported and might explain the low plasma stability of compounds **14** and **23**.[47] The corresponding (R)-azetidine **24** was less potent than **23** in the blood assay. The N-methylated analogue of **18** (**25**) was nearly 5-fold more potent than **14** in the blood BCR/CD69 assay and displayed 94 % BTK occupancy. Increasing the length of the open chain linker to three carbons led to **26** which was significantly less potent than **25** in the blood assay. Modifying the N-methyl substituent on the acrylamide to an ethyl

group provided **27**, which was comparable to **25** with respect to blood potency and target occupancy. However, **27** had a higher logP compared to **25** (3.6 vs 2.9) and interestingly inhibited CYP2D6 with an IC_{50} of 1.26 μM. Overall, **27** did not seem to offer any advantage over **25**. With the exception of azetidine acrylamide **23** all compounds from Table 2 tested for stability in human plasma showed plasma half-lives of >120 min.

Table 2. Linker modifications.

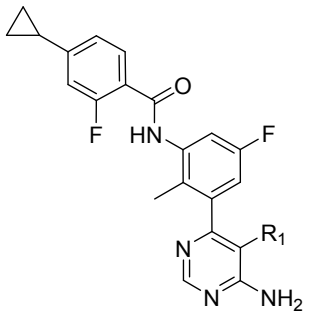

	R_1	BTK IC_{50} (nM)[a]	FcγR/IL8 IC_{50} (nM)[b]	BCR/CD69 IC_{50} (nM)[c]	Permeability logPe pH 6.8[d]	Stability in human plasma, $t_{1/2}$ [min]	BTK occupancy [%] after a 3 mg/kg dose[e]
17	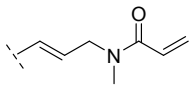	1.9 ± 1.2	11 ± 3	44 ± 4	-4.5	>120	77
18	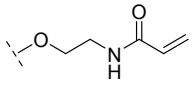	8.7 ± 4.6	18 ± 13	105 ± 13	-5.4	>120	84
19	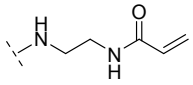	51 ± 38	671 ± 690	1245 ± 350	-5.8	n.t.	n.t.
20	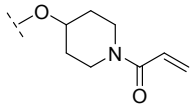	3.7 ± 4.5	12 ± 2	201 ± 63	-4.5	>120	77
21	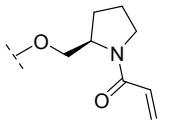	1290 ± 916	1869 ± 87	n.t.	-3.9	n.t.	n.t.
22	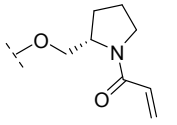	1.4 ± 0.4	9[f]	57 ± 8	-4.1	>120	90
23	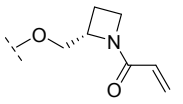	3.1 ± 0.5	5[f]	50 ± 3	-3.9	42	80
24	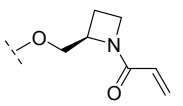	7.5 ± 6.3	60 ± 14	354 ± 59	-4.1	n.t.	n.t.

25	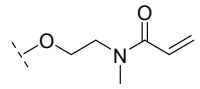	1.3 ± 0.9	2.5 ± 0.7	18 ± 5	-4.3	>120	94
26	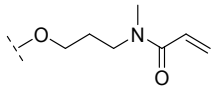	3.6 ± 1.3	17 ± 6.5	91 ± 9	-4.0	n.t.	n.t.
27	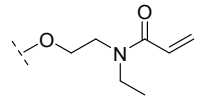	0.9 ± 0.2	5[f]	28 ± 4	-4.2	>120	93

a) BTK enzyme IC_{50} shown as means ± SD (n ≥ 2); b) FcγR induced IL8 IC_{50} shown as means ± SD (n ≥ 2); c) anti-IgM/IL-4 induced CD69 expression on human blood B cells IC_{50} shown as means ± SD (n ≥ 2); d) PAMPA permeability, logPe at pH 6.8; e) BTK occupancy in rat spleen homogenate 5 h after po dose of compounds compared to vehicle control, determined as mean (n = 3); f) n = 1; g) n.t.: not tested.

Having identified the highly potent acrylamide **25**, we wanted to assess if an alternative warhead could provide an overall advantage. Generally, a highly reactive moiety could lead to increased binding to off-targets, whereas too low intrinsic reactivity could lower the reaction rate to the Cys of interest. To probe the intrinsic reactivity of different warheads we investigated the stability of the compounds towards an excess of glutathione (GSH) as a surrogate for Cys-containing nucleophiles and proteins (Table 3). In the presence of GSH, **25** showed a slow decrease with 68.5 % remaining parent after 24 h. For the sterically hindered methyl substituted acrylamide **28**, a significantly decreased reactivity towards GSH was observed. However, **28** was also significantly less active in the blood BCR/CD69 assay. The 4-(dimethylamino)but-2-enamide **29** showed a slow decrease in the presence of GSH over 24 h, similar to **25**. However, the permeability of **29** was very low (log Pe pH 6.8 <-6.5) and together with the reduced blood BCR/CD69 potency compared to **25** we did not pursue this compound further. The propynamide **30** was highly unstable in the presence of GSH with complete disappearance of the parent within 24 h. In addition, only limited stability ($t_{1/2}$ 96 min) in human plasma was observed. For the but-

2-yneamide **31**, decrease of parent was slow, but due to the decreased blood BCR/CD69 assay potency this compound was also not considered further. In summary, compound **25** (LOU064, remibrutinib) exhibited the best overall profile and was selected for further characterization.

Table 3. Warhead modifications.

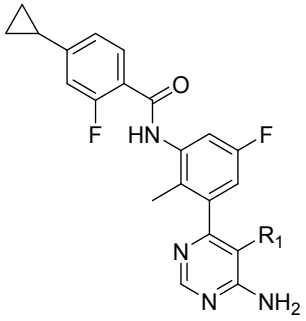

	R_1	BTK IC_{50} (nM)[a]	FcγR/IL8 IC_{50} (nM)[b]	BCR/CD69 IC_{50} (nM)[c]	Stability in presence of GSH at 24 h[d]
25	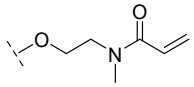	1.3 ± 0.9	2.5 ± 0.7	18 ± 5	68.5
28	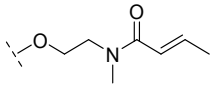	104 ± 77	263 ± 119	983 ± 617	95.8
29	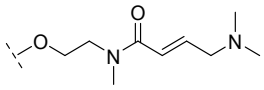	11 ± 5	76 ± 3	151 ± 69	60.8
30	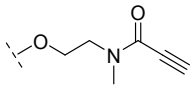	1.8 ± 0.2	6.5 ± 2	49 ± 23	0.1
31	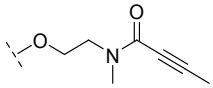	5.2 ± 2	32 ± 7	161 ± 44	79.6
32	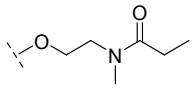	1’300 ± 424	>10’000	>20’000	n.t.

a) BTK enzyme IC_{50} shown as means ± SD ($n \geq 2$); b) FcγR induced IL8 IC_{50} shown as means ± SD ($n \geq 2$); c) anti-IgM/IL-4 induced CD69 expression on human blood B cells IC_{50} shown as means ± SD ($n \geq 2$); d) The stability in the presence of GSH is given as ratio area (analyte/internal standard) in %; e) n.t.: not tested.

The melting point of crystalline LOU064 is 194 °C. It has a low thermodynamic solubility of <0.003 g/L at pH 6.8, but solubility increases to >1.5 g/L at pH 1. The permeability is high (PAMPA: log Pe pH 6.8 -4.3; Caco Papp(A-B) 15.9, Papp(B-A) 10.2) suggesting good absorption. The half-maximum inhibition of the CYP enzymes 3A4, 2C9 and 2D6 was ≥ 5 μM (see Supporting Information). LOU064 showed some activity in an *in vitro* PXR reporter gene assay (EC_{50} >5.48 μM and E_{max} 94.7 %) indicating a risk for CYP induction and drug-drug interactions.

LOU064 Binds Covalently to BTK. The covalent character of BTK inhibition by LOU064 was confirmed in a series of studies. First, the kinetics of BTK inhibition were assessed in an enzyme dilution experiment.[48] The biochemical BTK enzyme assay (Supporting Information) was modified to include a one hour preincubation of BTK protein at a concentration of 4.7 μM with a 10 % molar excess of compound. The compound/enzyme mixture was then diluted into kinase assay buffer containing ATP and peptide substrate to reach a final concentration of 1 nM BTK and 1.1 nM compound and enzyme activity was monitored by measuring substrate phosphorylation (Figure 4). The increase in phosphorylated substrate peptide over time indicated recovery of BTK kinase activity by the dilution step for the DMSO solvent control, the reversible BTK inhibitor staurosporine, as well as the inactive non-covalent ethylamide analog **32** (Table 3). In line with expectations for a covalent binder, LOU064 showed no recovery of BTK activity after the dilution step.

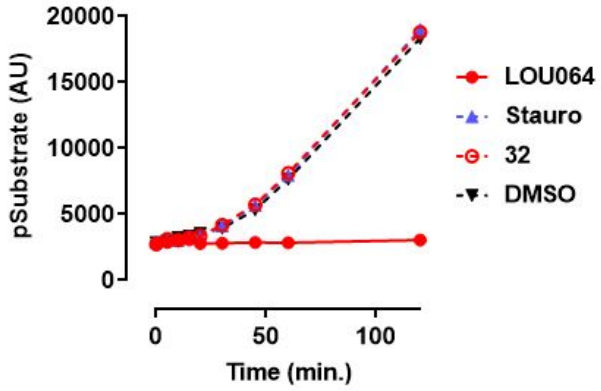

Figure 4. Rescue of BTK enzymatic activity by dilution. The increase of phosphorylated substrate peptide over time after the dilution step is indicated for the DMSO solvent control (black dash and triangles), for the reversible BTK inhibitor staurosporine (blue dash and triangles), for the non-covalent ethylamide analog **32** (red dash and empty circles) and for LOU064 (red line and filled circles).

Secondly, we assessed covalent binding of LOU064 to the BTK kinase domain by analysis with LC/MS (Experimental details see Supporting Information), which revealed the presence of a main peak with 32'222.3 Da mass, closely corresponding to the predicted BTK/LOU064 1:1 adduct (based on the masses of 507.5 and 31'714.5 Da, respectively for LOU064 and the kinase domain construct). This provided further evidence for a specific and single covalent modification of BTK by LOU064 (Figure 5).

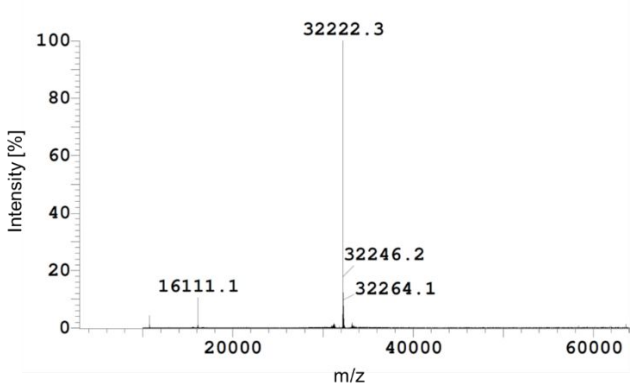

Figure 5. Deconvoluted mass spectrum of covalent BTK kinase domain (encompassing amino acids 386-659) adduct with LOU064. The peak with a corresponding mass of 32222.3 Da is indicative of the presence of one covalent adduct of LOU064 (507.5 Da) to the BTK kinase domain (31'714.5 Da).

Thirdly, solving the complex structure revealed the atomic details of LOU064 binding to BTK and confirmed the design hypothesis. As expected, the inhibitor is covalently attached to Cys481 (Figure 6), with the carbonyl of the acrylamide making a hydrogen bond with the NH of the backbone of Cys481. The amino-pyrimidine moiety forms a bidentate hydrogen bonding interaction with the backbone of Met477 of the kinase hinge region. The phenyl group of LOU064 at position 4 of the 6-aminopyrimidine scaffold makes hydrophobic contacts with the Val416 side chain while the fluorine makes a multipolar interaction with the carbonyl of Gly409 of the Gly-rich loop (Figure S-1, Supporting Information).[49] The fluoro-phenyl-cyclopropyl-group occupies the H3 pocket and stabilizes it in an inactive state. The H3 pocket[16] is formed by the side chains of Gln412, Phe413 (both Gly-rich loop), Asp521, Asn526 (both part of the catalytic loop), Asp539 (DFG), Leu542, Ser543, Val546, and Tyr551 (belonging to the activation loop) (Figure S-1). The

fluorine in this pocket points towards the cavity, instead of towards the NH of the amide of the ligand, most likely to avoid the unfavorable vicinity to the carbonyl of Asn526 (Figure S-1) .

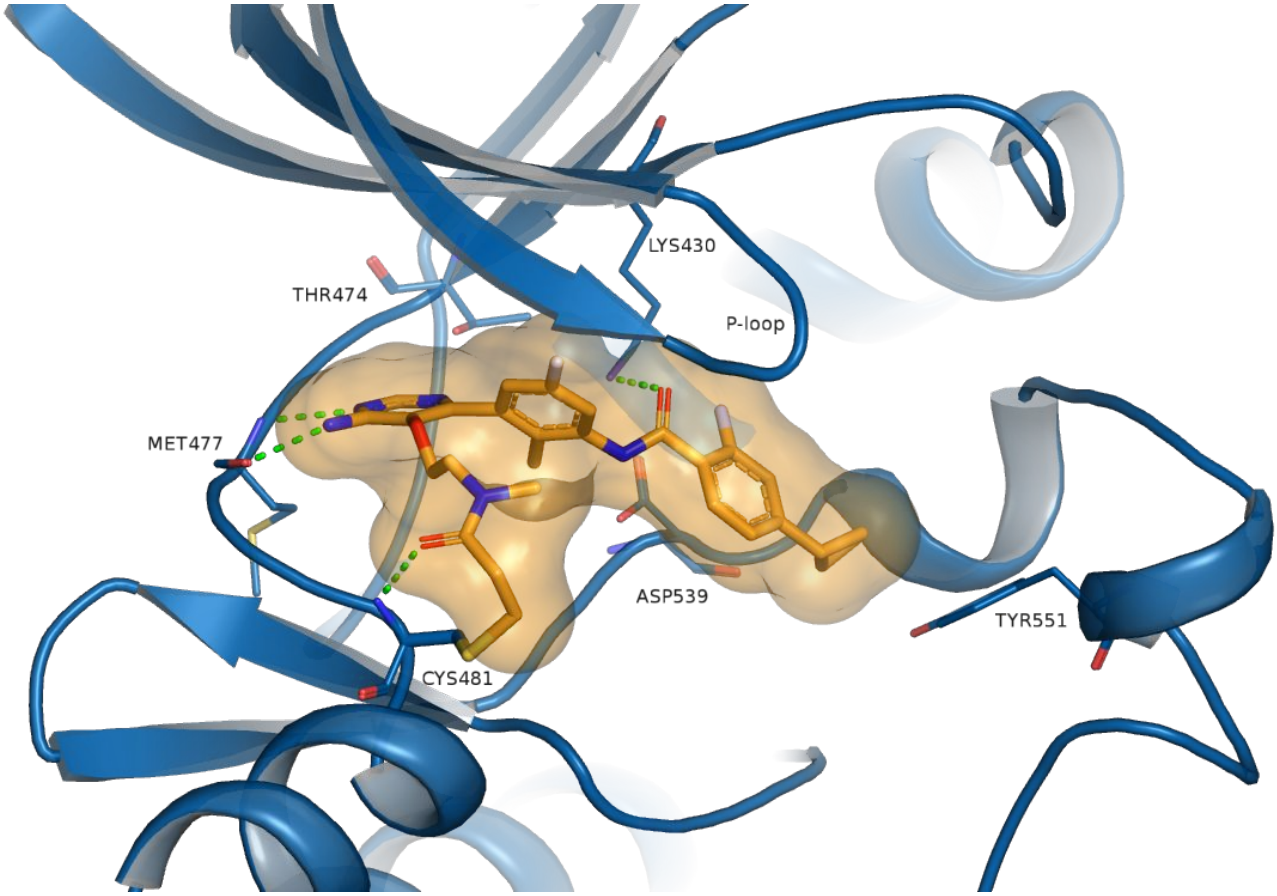

Figure 6. X-ray complex structure of BTK kinase domain bound to LOU064 (PDB 6TFP, protein chain A with ligand chain L). The molecular surface of LOU064 is colored in orange and key residues lining up the binding site are shown as labelled stick model. The main polar interactions between protein and inhibitor are indicated with dotted green lines. For improved clarity water molecules are omitted.

Selectivity of LOU064. Our aim was to combine covalent BTK binding and the high selectivity associated with binding to the inactive BTK conformation. The selectivity of LOU064 was assessed not only in a selected panel of enzymatic kinase assays, but also in a competition binding

assay[50] against 395 human non-mutant kinases and 61 atypical, mutant or pathogen kinases. In this screen (KINOMEscan™, DiscoverX), LOU064 at a concentration of 1 μM showed full inhibition of probe binding to BTK (0.25 % remaining probe binding) and partial inhibition of TEC (24 % remaining probe binding) and BMX (53 % remaining probe binding), indicating an excellent kinase selectivity profile (TREE*spot*™ Kinase Dendogram of LOU064 (Figure S-2) and KINOMEscan data in Supporting Information).

Based on this kinome-wide screen, the selectivity of LOU064 was further assessed and compared to clinical covalent BTK inhibitors. As the determination of IC_{50} values in biochemical enzyme assays for covalent inhibitors suffers from time-dependent effects[48] we determined the binding constants (K_d) in a competition binding assay[50,51] for a set of Cys-containing kinases (Table 4). LOU064 showed very potent affinity to BTK with a subnanomolar K_d of 0.63 nM and with a selectivity of 175 fold against TEC (K_d of 110 nM) and 857 fold against BMX (K_d of 540 nM). LOU064 did not show binding to ITK, EGFR, ERBB2, ERBB4 and JAK3 up to 10 μM. By contrast, ibrutinib (**1**) showed similar high affinity for BTK, but poor selectivity against BMX, TEC, EGFR, ERBB2 and ERBB4. Of note, acalabrutinib (**2**), tirabrutinib (**3**) and evobrutinib (**4**) are significantly less potent than LOU064 on BTK and less selective. Branebrutinib (**5**) displayed high affinity for BTK, comparable to LOU064 and ibrutinib, with an improved selectivity profile compared to ibrutinib, however inferior to LOU064, potently inhibiting BMX and TEC. These binding data are in line with recent publications in other assay systems[39] and our data in biochemical enzyme assays (not shown). Overall, in addition to being amongst the most potent inhibitors for BTK, LOU064 differentiates with its excellent, best-in-class kinase selectivity from other clinical-stage covalent inhibitors.

Table 4. Binding constants (K_d in nM) of covalent BTK inhibitors for selected kinases containing a conserved cysteine and selectivity vs off-target kinases ($K_{d,\ off\text{-}target}/K_{d,\ BTK}$).

		BTK	BMX	TEC	ITK	EGFR	ERBB2	ERBB4	JAK3
25 (LOU064)	K_d	0.63	540	110	>10000	>10000	>10000	>10000	>10000
	Fold	1	857	175	>15873	>15873	>15873	>15873	>15873
1 (ibrutinib)	K_d	1.9	1.6	1.7	57	6.9	1.2	2.4	37
	Fold	1	0.6	0.9	30	3.6	0.6	1.3	19
2 (acalabrutinib)	K_d	21	610	14	>10000	5600	7.4	140	>10000
	Fold	1	29	0.7	>476	267	0.4	6.7	>476
3 (tirabrutinib)	K_d	14	47	6.2	>10000	>10000	610	>10000	>10000
	Fold	1	3.4	0.4	>714	>714	44	>714	>714
4 (evobrutinib)	K_d	16	31	4.5	3700	7100	>10000	5600	>10000
	Fold	1	1.9	0.3	231	443	>625	350	>625
5 (branebrutinib)	K_d	0.56	22	0.99	320	>10000	>10000	2500	1300
	Fold	1	39	1.8	571	>17857	>17853	4464	2321

We evaluated the cellular selectivity of LOU064 in a panel of culture systems with primary human cells representative for several tissues, including fibroblasts, epithelial cells, keratinocytes and immune cells (BioMAP Diversity plus panel, DiscoverX).[52] LOU064 was tested at concentrations of 270, 900, 3000 and 10000 nM, all concentrations well above its cellular BTK inhibition in cell culture conditions (Figure S-3, Supporting Information). The main activity

detected was in the BT panel, and represents the intended inhibition of cellular BTK function in B cells stimulated via the B cell receptor and in the presence of T cell co-stimulatory pathways, resulting in the inhibition of several inflammatory readouts such as TNF-α, IL-17A, IL-6 and IL-2, as well as inhibition of B cell proliferation (indicated by the gray arrow in the BT panel). The response was not concentration dependent as all concentrations tested were well above maximal cellular BTK inhibition. Of note is the absence of a peak in the EGFR signal in the HDF3CGF panel, clearly indicating the lack of any activity of LOU064 in the dermal fibroblast system, an effect which has been shown for BTK inhibitors with off-target effects on EGFR, such as ibrutinib (Figure S-4, Supporting Information).[22] Across all these cellular systems, LOU064 showed no cytotoxicity. In addition to the expected effects on B cell proliferation, LOU064 exerted effects on fibroblast proliferation at concentrations of 270 and 10000 nM (gray arrow in the HDF3CGF panel).

Furthermore, the high selectivity of LOU064 was confirmed by testing against a broad panel of *in vitro* assays (in binding or in functional mode) comprising 85 G-protein coupled receptors, transporters, nuclear receptors, enzymes and ion channels (Supporting Information). LOU064 did not show binding, inhibition, or activation in any of these assays at concentrations up to 10 μM, with the exception of PIK4CB (IC_{50} 3.1 μM) and Bile Salt Export Pump (BSEP, IC_{50} 6.6 μM), thus establishing a more than 2000-fold selectivity for BTK over these off-targets. In the *in vitro* hERG patch clamp assay an IC_{50} of 1.4 μM was measured. In preclinical invasive and non-invasive dog telemetry studies after single and long-term dosing, no effect on any cardiovascular parameter was detected. As the non-covalent analog **32** showed very similar activity on BSEP (IC_{50} 3.7 μM) and hERG (IC_{50} 2.9 μM in Qpatch assay), it is likely that the interaction of LOU064 with these off-target proteins is non-covalent. No significant inhibition of other cardiac

ion channels (Nav1.5, Cav1.2, KCNQ1) was observed and LOU064 was found negative in genotoxicity and mutagenicity assays (*in vitro* Ames, *in vitro* and *in vivo* micronucleus tests). Similarly, LOU064 was negative in the 3T3 NRU phototoxicity assay.

Preclinical PK Profile of LOU064. The *in vitro* clearance of LOU064 in microsomes was moderate in rat, and high in mouse and dog (Table 5). The *in vivo* pharmacokinetic properties of LOU064 were assessed in rat, mouse and dog (Table 5). In rats, the compound displayed a moderate clearance, a low volume of distribution, a short half-life, and a moderate bioavailability. LOU064 was mainly cleared via oxidative metabolism and elimination of unchanged LOU064 was not a major pathway in rat. In mice, LOU064 displayed a similar PK profile as for rats with high CL, a low volume of distribution and a short half-life. In dogs, the clearance was high, in the range of the hepatic blood flow, the volume of distribution was low, the half-life was short and the bioavailability was low. Formulations were developed which enabled preclinical toxicology studies to be carried out (not shown).

Table 5. *In vitro* and *in vivo* pharmacokinetic parameters of LOU064 in rat, mouse and dog

	Rat	Mouse	Dog
In vitro CL int (μL/min/mg)	33	325	146
Hepatic extraction (%)	52	93	87
In vivo	Female Lewis	Female C57BL/6	Male Beagle
Dose	1 mg/kg iv	1 mg/kg iv	1 mg/kg iv

	3 mg/kg po	3 mg/kg po	3 mg/kg po
CL (mL / min / kg)	44 ± 12	97 ± 11	29 ± 4
V_{ss} (L / kg)	1.4 ± 0.3	1.0 ± 0.1	1.0 ± 0.1
$t_{1/2}$ (h)	0.5 ± 0.03	1.0 ± 0.1	0.9 ± 0.1
C_{max} d.n. (nM)	148 ± 33	53 ± 14	19
T_{max} (h)	0.3	0.3 ± 0.1	0.8
F (%)	29 ± 3	16 ± 4	5
AUC po d.n. (nM · h)	225 ± 27	54 ± 15	55

In essence, the preclinical ADME properties of LOU064 are characterized by excellent permeability, high clearance and fast elimination.

***In vitro* BTK Inhibition Kinetics.** To further characterize the mechanism of BTK inhibition by LOU064, we tested the kinetics of enzymatic inhibition. In biochemical assays of enzymatic activity with recombinant full-length human BTK, LOU064 showed very fast inhibition of BTK (Figure S-5, Supporting Information). LOU064 showed potent BTK inhibition starting from the earliest time-point and no indication of a time-dependent shift in IC_{50} over the timeframe that allowed reliable detection of BTK activity or inhibition. The very fast binding kinetics of LOU064 to purified BTK prevented the determination of accurate and meaningful biochemical reaction parameters.

We therefore assessed the engagement of cellular BTK in a clinically relevant matrix - human blood. Blood from healthy volunteers was mixed with serial dilutions of LOU064, incubated at

room temperature to allow binding to cellular BTK and at given time points, aliquots of blood were sampled and analyzed for covalent binding of LOU064 to BTK with immunoassays for free BTK (i.e. not covalently occupied by compound) and total BTK protein (see Supporting Information). LOU064 showed very rapid covalent binding to cellular BTK in human blood at concentrations as low as 300 nM (Figure 7, left panel).

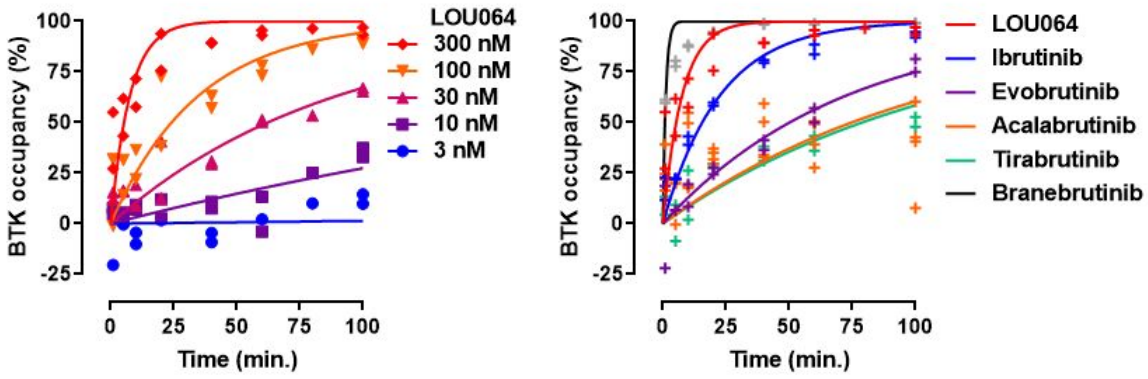

Figure 7. Time- and concentration-dependent *in vitro* engagement of cellular BTK by LOU064 and related inhibitors in human blood. Left panel shows data for LOU064 from two independent experiments with different blood donors (solid lines show non-linear one-phase association curve fits). Right panel shows the association kinetics for a concentration of 300 nM for each compound (solid lines show non-linear one-phase association curve fits). Individual data from two independent experiments with different blood donors.

We compared the binding characteristics of LOU064 to related covalent BTK inhibitors in the same type of assay at a concentration of 300 nM (Figure 7, right panel). In contrast to the rapid and complete BTK binding of LOU064, the other covalent BTK inhibitors, with exception of branebrutinib, showed slower binding kinetics. A comparison of the enzymatic and cellular

potency of LOU064 to these covalent BTK inhibitors across several assays confirmed the very high potency of LOU064 (Table 6). These data suggest that LOU064 has very fast reaction kinetics and rapidly reaches full BTK inhibition in relevant matrices such as human blood.

Table 6. Comparative potency of LOU064 and covalent BTK inhibitors

	BTK IC_{50} (nM)[a]	FcγR/IL8 IC_{50} (nM)[b]	BCR/CD69 IC_{50} (nM)[c]	FcεR/CD63 IC_{50} (nM)[d]
LOU064 (**25**)	1.3 ± 0.9	2.5 ± 0.7	18 ± 5	67 ± 54
Ibrutinib (**1**)	2.3 ± 2	16 ± 14	66 ± 57	230 ± 210
Acalabrutinib (**2**)	19 ± 22	24 ± 24	203 ± 77	747 ± 75
Tirabrutinib (**3**)	5.2 ± 5	26 ± 16	132 ± 46	363 ± 200
Evobrutinib (**4**)	62 ± 4	61 ± 37	320 ± 74	1182 ± 819
Branebrutinib (**5**)	0.1 ± 0.05[18]	6.0 (n = 1)	18 ± 4	40 ± 10

a) BTK enzyme inhibition in Caliper assay IC_{50} shown as means ± SD ($n \geq 2$); b) FcγR induced IL8 IC_{50} shown as means ± SD ($n \geq 2$); c) anti-IgM/IL-4 induced CD69 expression on human blood B cells IC_{50} shown as means ± SD ($n \geq 2$); d) anti-IgE-induced degranulation and CD63 expression on human blood basophils.

***In vivo* BTK Engagement.** For a covalent inhibitor of BTK, the PD effects are determined by the extent and duration of BTK target occupancy. The initial inactivation of BTK by LOU064 binding is primarily determined by the systemic exposure of the drug. Once the drug is eliminated from systemic circulation the duration of BTK inhibition becomes independent from drug exposure and is determined by the turnover of the inactive drug/protein complex by synthesis of new BTK protein.[53] For BTK, the turnover of inactivated protein by newly synthesized protein has been described in preclinical models and ranges from 20 – 40 % of BTK protein being resynthesized after 24 h.[18,22,54]

We set out to determine the detailed PK/PD relationship of LOU064 in rats by using BTK occupancy as the primary PD readout. A series of studies were performed in rats to determine the dose range leading to varying degrees of BTK occupancy in spleen (Figure 8). To minimize the impact of circulating LOU064, the animals were killed 5 hours after oral dosing and tissues were sampled. BTK occupancy in spleen homogenates was measured relative to vehicle controls. A dose-response curve fit indicates an EC_{50} of 0.6 mg/kg (EC_{90} 1.6 mg/kg). The analysis of LOU064 in blood from these animals showed that for the 1 mg/kg dose, resulting in an average of 78 % BTK occupancy, the systemic exposure was 49.1 nM at 0.5 hours post dose (5.6 nM at 5 hours). This suggests that very low and transient systemic exposures of LOU064 are sufficient for BTK inhibition.

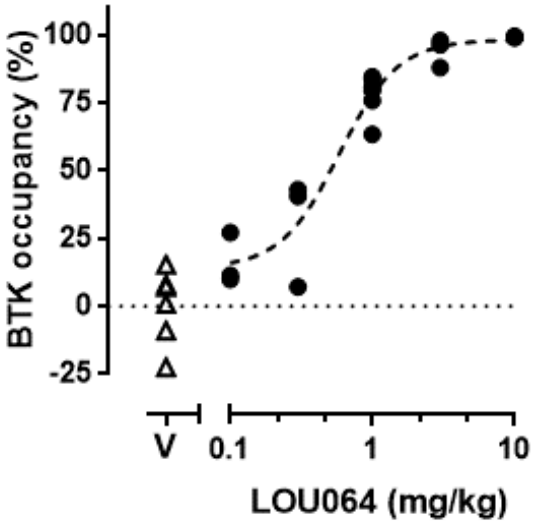

Figure 8. Spleen BTK occupancy relative to vehicle controls was measured 5 hours after oral dosing in female rats combined from two separate studies (with 3 animals per each dose group). Open triangles show the BTK occupancy levels in the combined vehicle dosed animals. Filled

circles show the BTK occupancy of LOU064 treated animals. The dotted line shows a dose-response curve fit.

Preclinical Efficacy in SRBC and CIA Models. To extend the preclinical PK/PD relationship to repeated dosing regimen, we examined the efficacy of LOU064 in a model of B cell dependent antibody formation following immunization with sheep red blood cells (SRBC).[55] Female rats were immunized with SRBC and treated for 4 days with one daily oral dose of LOU064 starting on the day of immunization. On day 5, SRBC antibody formation was assessed *ex vivo* on splenocytes, as well as BTK occupancy in the same tissue (Figure 9, left panel). The IgM antibody response was maximally inhibited (by 96 %) at a dose of 3 mg/kg q.d.. This level of IgM response inhibition was correlated to a spleen BTK occupancy at the 24 h trough of 71.5 % (Figure 9, right panel). Doses as low as 0.3 mg/kg demonstrated a partial, but significant inhibitory effect on SRBC specific antibody response (with a trough BTK occupancy in spleen of 31 %).

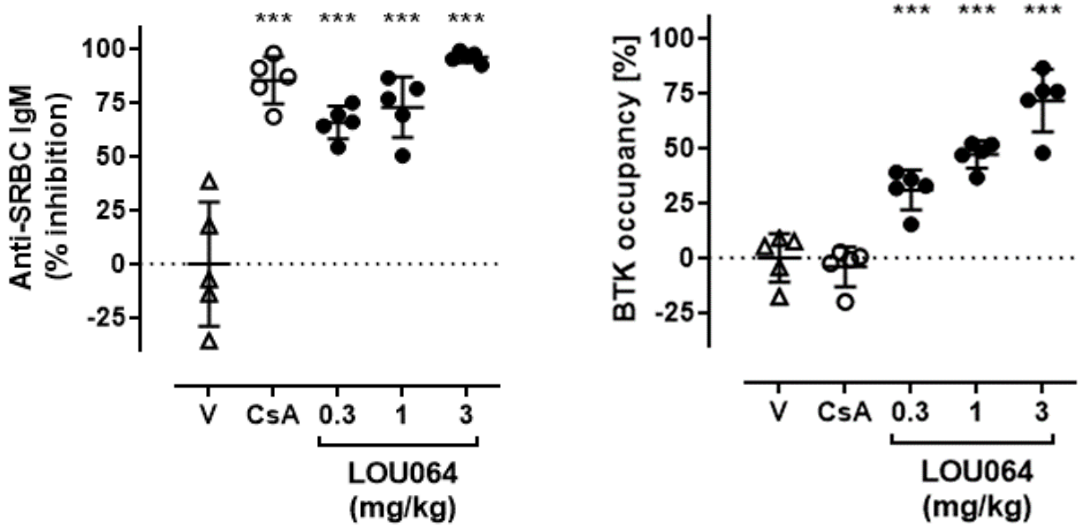

Figure 9. IgM response inhibition by LOU064 in the rat model of B cell response to SRBC immunization. Left panel: inhibition of anti-IgM response: open triangles show vehicle (V), open circles cyclosporine A (CsA) and closed circles LOU064 treated animals, respectively. The group means are shown as the central bars and the standard deviations are shown as whisker error bars. Statistical significance (ANOVA, followed by Dunnett's test) is shown as *** for $p < 0.001$. Right panel: BTK occupancy in spleen 24 hours after the last dose of LOU064: open triangles show vehicle (V), open circles cyclosporine A (CsA) and closed circles LOU064 treated animals relative to the average of the vehicle group. Group means are shown as central bars and standard deviations as whisker error bars. Statistical significance (ANOVA, followed by Dunnett's test) is shown as *** for $p < 0.001$.

Next we assessed the effects of LOU064 in the inflammatory model of collagen-induced arthritis (CIA) in rats.[56,57] Collagen-specific B- and T-lymphocytes are important in the pathogenesis of CIA, with the peak of the T-cell response occurring around the time of disease onset.[57,58] Female Lewis rats were immunized with porcine collagen and LOU064 oral dosing, once daily, was started after the onset of arthritis, continuing until day 26 after immunization. The animals treated with LOU064 showed a fast onset of action and within a few days paw swelling was fully reduced (Figure 10, left panel). This was evident in the three highest doses of 3, 10 and 30 mg/kg, whereas the 0.3 mg/kg dose was largely inactive (no 1 mg/kg dose group was included in the study).

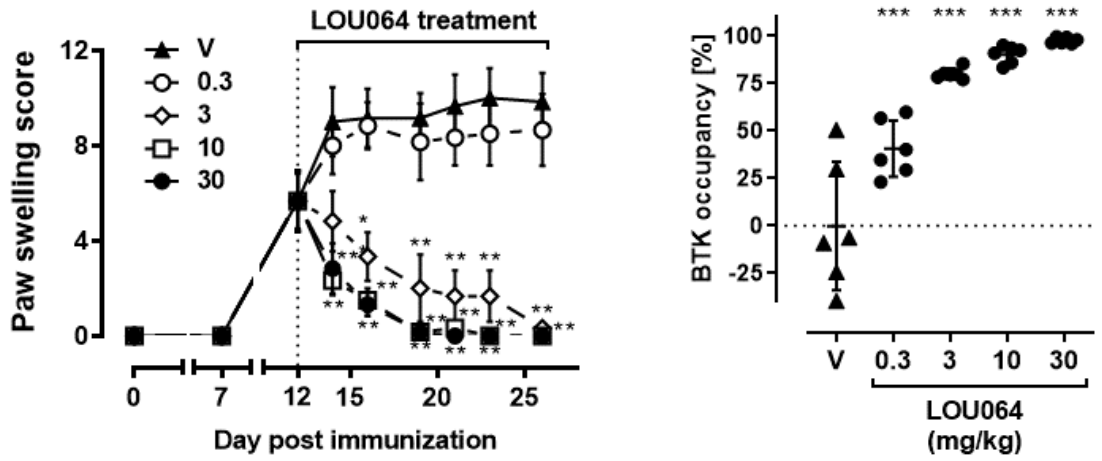

Figure 10. Efficacy of LOU064 in the rat model of collagen-induced arthritis. Left panel: Paw swelling scores are shown as means ± SEM. LOU064 treatment once daily with doses of 0.3, 3, 10 and 30 mg/kg from day 12 to 25 post immunization. Statistical significance (ANOVA, followed by Dunnett's test) is shown as ** $p < 0.01$. Right panel: BTK occupancy in spleen 24 hours after the last dose of LOU064. Triangles show vehicle (V) and circles represent LOU064 treated animals relative to the average of the vehicle group. Group means are shown as central bars and standard deviations as whiskers. Statistical significance (ANOVA, followed by Dunnett's test) is shown as *** $p < 0.001$.

Histopathological analysis of the 3 and 10 mg/kg groups showed that bone and cartilage erosion, as well as inflammatory cell infiltration, were all significantly inhibited by LOU064 (Figure 11). Dose proportional levels of BTK occupancy in spleen were found on day 26 at trough, 24 hours after the last dose (Figure 10, right panel). Occupancy levels of 80 % (for the 3 mg/kg dose) and higher were associated with significant inhibition of paw swelling.

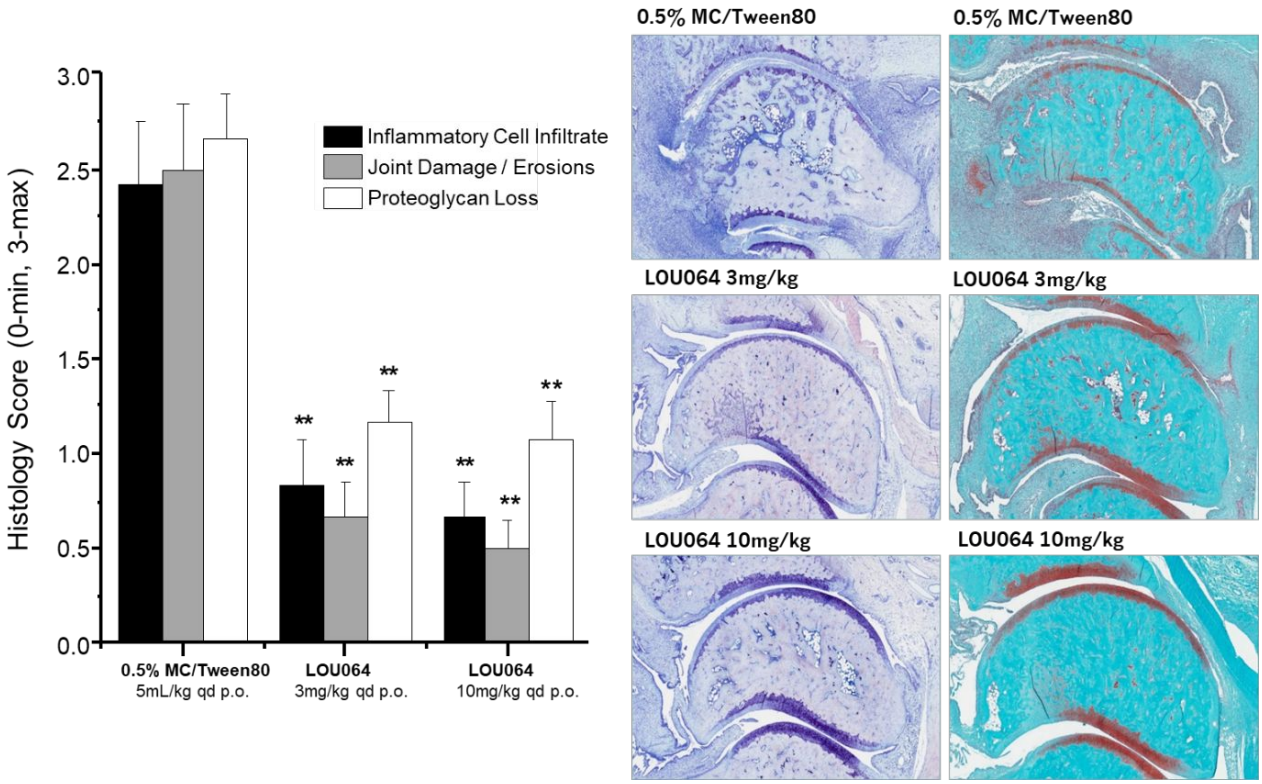

Figure 11. Histopathological analysis of arthritis in rat CIA model. Left panel: Histology scores combined for the hind paws of each animal show inflammatory cell infiltrate, joint damage and proteoglycan loss (average +/- SEM of 6 animals per group, ANOVA, followed by Dunnett's test ** for $p < 0.01$). Right panel: Photomicrographs of paw sections stained with Giemsa (left column) and Safranin O (right column) illustrate joint tissue inflammation and preservation of joint cartilage, respectively. LOU064 significantly reduced join inflammation and damage as well as proteoglycan loss at 3 and 10 mg/kg q.d. po.

This study shows that LOU064 potently inhibits a chronic arthritic inflammation *in vivo* in a therapeutic treatment setting with a fast onset of action. Since we timed the treatment to start

after immunization phase, the fast onset of action suggests that the anti-inflammatory effect is due to the inhibition of inflammatory macrophages and of immune complexes in the paws.

Synthesis of LOU064 (25). The synthesis of **25** is outlined in Schemes 1 and 2. Scheme 1 shows the synthesis of the upper portion of the molecule, intermediate **38**. Borylation of 1-bromo-5-fluoro-2-methyl-3-nitrobenzene (**33**) with bis(pinacolato)diboron in the presence of Pd(dppf)Cl_2·DCM and potassium acetate gave boronic ester **34** which upon catalytic hydrogenation provided aniline **35**. Suzuki reaction of methyl 4-bromo-2-fluorobenzoate (**36**) and cyclopropylboronic acid gave cyclopropyl intermediate **37**. Boronic ester **38** was then accessed via a NaHMDS mediated amide formation of aniline **35** and ester **37**. The synthesis of LOU064 was completed as outlined in Scheme 2. The lower portion of the molecule was assembled starting from 2,4-dichloro-3-methoxypyrimidine (**39**). Treatment with ammonia in a pressure reactor resulted in aminopyrimidine **40**, which was subjected to boron tribromide treatment to give amino-pyrimidinol **41**. The linker moiety was introduced via a Mitsunobu reaction with N-Boc-N-methyl-2-hydroxyethylamine in the presence of DIAD and Smopex-301, a convenient polymer supported version of triphenylphosphine, to obtain **42**. Boc protected intermediate **43** was assembled via Suzuki coupling of **42** and **38**. Finally, Boc deprotection of **43** followed by amide coupling with acrylic acid in the presence of propylphosphonic anhydride (T3P) provided LOU064 (**25**).

The experimental details are provided in the Experimental Section. For the synthesis of analogues the schemes and synthetic details are provided in the Supporting Information.

Scheme 1. Synthesis of boronic ester **38**.[a]

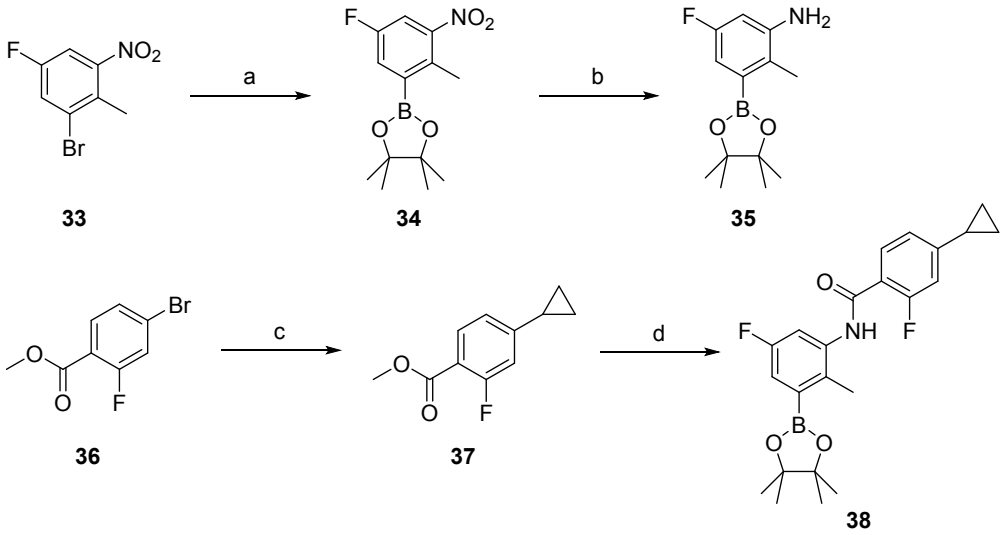

[a]Reagents and conditions: (a) BISPIN, $Pd(dppf)Cl_2 \cdot DCM$, KOAc, dioxane, 100 °C, 3.5 h, 92 %; (b) H_2, Pd/C, MeOH, RT, 7 h, 93 %; (c) cyclopropylboronic acid, $Pd(OAc)_2$, tricyclohexylphosphine, K_3PO_4, water, toluene, 100 °C, overnight, 99 %; (d) **35**, NaHMDS (1 M in THF), THF, RT, 4 h, 76 %.

Scheme 2. Synthesis of LOU064.[a]

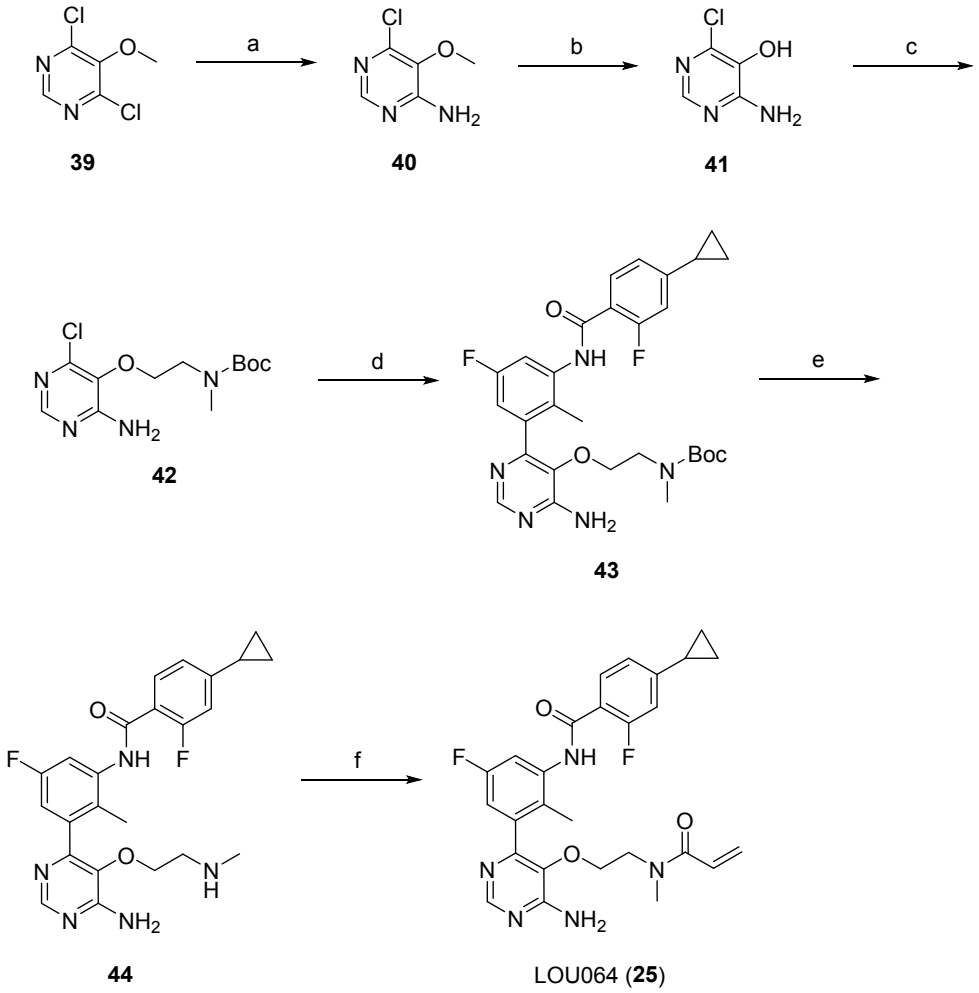

[a]Reagents and conditions: (a) NH_4OH, 2-propanol, 70 °C, 48 h, 94 %; (b) BBr_3, DCM, 40 °C, 3 h, 59 %; (c) N-Boc-N-methyl-2-hydroxyethylamine, DIAD, Smopex-301, THF, 60 °C, 2 h, 53 %; (d) **38**, $Pd(PPh_3)_2Cl_2$, aq. Na_2CO_3, DME, water, microwave, 110 °C, 25 min, 74 %; (e) TFA, DCM, RT, 12 h; (f) acrylic acid, DIPEA, T3P (50 % in DMF), DMF, RT, 2 h, 45 % over 2 steps.

Conclusions

In summary, we have discovered a covalent BTK inhibitor, LOU064 (remibrutinib, **25**), that shows excellent selectivity and potency with potential for best-in-class *in vivo* profile. By a

structure-based approach, starting from a selective, reversible BTK binder, we successfully morphed the hinge binder moiety and introduced a linker with a warhead leading to selective, covalent BTK inhibitors. The drug discovery efforts focused on the optimization of potency, ADME properties and PK/PD using an *in vivo* target occupancy assay.

The preclinical pharmacokinetic data of LOU064 is favorable for a covalent inhibitor with the potential for once daily dosing. Based on the singular PK/PD profile of a covalent inhibitor LOU064 showed potent BTK occupancy with an EC_{90} of 1.6 mg/kg after single oral dose with transient low exposure. In addition, the *in vivo* efficacy on B cell response and the potent inhibition of rat arthritis with a fast onset of action suggest that the compound could have utility in treating autoimmune diseases. The compound displayed a good preclinical tolerability and safety profile in two species at different doses and these findings encouraged us to progress LOU064 into clinical studies in autoimmune diseases. In phase I studies, healthy and atopic subjects have been exposed to LOU064 at doses ranging from 0.5 mg to 600 mg.[59] Administration of LOU064 in healthy subjects did not raise any safety signals in any of these studies. With favorable phase I results, LOU064 entered phase 2 clinical studies in several immune disorders including chronic spontaneous urticaria and Sjoegren's Syndrome. Further details and clinical results will be reported in due course.

EXPERIMENTAL SECTION

Experimental Details

All chemicals were used directly as received from commercial suppliers. ^{1}H NMR and ^{13}C NMR spectra were recorded on Bruker 400 or 600 spectrometers. Chemical shifts are expressed in δ ppm referenced to the residual solvent peak (DMSO-d6: δ = 2.50 ppm; $CDCl_3$: δ = 7.27 ppm; CD_3OD: δ = 3.30 ppm). Abbreviations used in describing peak signals are: br = broad signal, v = very, s = singlet, d = doublet, dd = doublet of doublets, t = triplet, q = quartet, m = multiplet. All final compounds were purified to > 95% by reverse phase high performance liquid chromatography (HPLC), supercritical fluid chromatography (SFC) or normal phase silica gel column chromatography. The purity was assessed by reverse phase UPLC with a gradient of 5–98 % acetonitrile in water (with either acid or base modifier) and monitored by UV absorption at 210-450 nM. Purity of all final compounds is ≥ 95 %. Low-resolution mass spectra were recorded on liquid chromatography-mass spectrometer in electrospray positive (ES+) and negative (ES-) mode. The HR-MS analyses were performed by using electrospray ionization in positive ion modus after separation by liquid chromatography (Nexera from shimadzu). The elemental composition was derived from the mass spectra acquired at the high resolution of about 30'000 on an LTQ Orbitrap XL mass spectrometer (Thermo Scientific). The high mass accuracy below 1 ppm was obtained by using a lock mass.

N-(3-(6-Amino-5-(2-(N-methylacrylamido)ethoxy)pyrimidin-4-yl)-5-fluoro-2-methylphenyl)-4-cyclopropyl-2-fluorobenzamide (**25**, LOU064). Step 1: To a solution of **43** (6.5 g, 11.74 mmol) in DCM (100 mL) was added TFA (9.05 mL, 117 mmol). The reaction mixture was stirred at RT for 12 h. The mixture was concentrated under reduced pressure. The residue was dried in vacuo to obtain the crude amine **44** as TFA salt. [ES-MS] (ESI+): m/z calcd for $C_{24}H_{26}F_2N_5O_2$ [M + H]+, 454.2; found, 454.3.

Step 2: To a solution of acrylic acid (1.10 g, 15.26 mmol) in DMF (50 mL) was added DIPEA (6.15 mL, 35.2 mmol) followed by T3P (50 % in DMF, 7.54 mL, 12.91 mmol). The mixture was stirred at RT for 30 min to form the active ester. The mixture was added dropwise to a solution of crude **44** and DIPEA (6.15 mL, 35.2 mmol) in DMF (50 mL) at 0 °C. The reaction mixture was stirred at RT for 2 h. The mixture was diluted with EtOAc and washed with water (2x) and brine. The organic layer was dried over $MgSO_4$, filtered and concentrated. The residue was purified by column chromatography (SiO_2; (DCM containing 2 % NH_3)/MeOH gradient) to afford 2.80 g of **25** as a white solid. Yield: 45 % over 2 steps. [ES-MS] (ESI+): m/z calcd for $C_{27}H_{28}F_2N_5O_3$ [M + H]+, 508.2; found, 508.3. ^{1}H NMR (500 MHz, DMSO-d_6) rotamers δ 9.79 and 9.57 (2s, total 1H), 8.22 and 8.19 (2s, total 1H), 7.78 – 7.72 and 7.71 – 7.65 (2m, total 1H), 7.63 – 7.52 (m, 1H), 7.15 – 7.03 (m, 4H), 7.03 – 6.96 (m, 1H), 6.71 – 6.57 (m, 1H), 6.14 – 6.02 (m, 1H), 5.65 – 5.56 (m, 1H), 3.63 – 3.54 (m, 2H), 3.54 – 3.45 (m, 2H), 2.81 and 2.51 (overlapping with DMSO) (2s, total 3H), 2.10 – 2.00 (m, 1H), overlapping with 2.03 and 1.98 (2s, total 3H), 1.11 – 1.03 (m, 2H), 0.86 – 0.78 (m, 2H). ^{13}C NMR (151 MHz, DMSO-d_6) rotamers δ 165.58, 165.54, 162.65, 162.40, 160.66, 160.50, 160.16, 160.04, 159.01, 158.85, 158.72, 158.56, 158.44, 153.84, 153.44, 153.35, 152.93, 151.06, 151.01, 150.82, 150.77, 138.75, 138.69, 138.34, 138.28, 137.85, 137.78, 137.70, 136.08, 135.23, 130.55, 130.36, 128.35, 128.32, 127.10, 126.89, 126.20, 126.05, 121.65, 121.59, 120.43, 120.34, 119.99, 119.90, 112.83, 112.78, 112.72, 112.63, 112.57, 112.22, 112.06, 111.86, 70.23, 68.69, 48.25, 47.36, 35.41, 32.80, 15.16, 14.23, 14.19, 10.55, 10.52. HRMS (ESI+): m/z calcd for $C_{27}H_{28}F_2N_5O_3$ $[M + H]^+$, 508.21547; found, 508.21582.

2-(5-Fluoro-2-methyl-3-nitrophenyl)-4,4,5,5-tetramethyl-1,3,2-dioxaborolane (34). To a solution of 1-bromo-5-fluoro-2-methyl-3-nitrobenzene (463 g, 1978 mmol) in dioxane was added bis(pinacolato)diboron (755 g, 2973 mmol) followed by potassium acetate (681 g, 6939 mmol)

and $PdCl_2$(dppf)·DCM adduct (85 g, 104 mmol). The reaction mixture was refluxed at 110 °C for 3.5 h. After cooling to RT the mixture was diluted with EtOAc and washed with saturated aqueous $NaHCO_3$ solution. The aqueous layer was back-extracted with EtOAc (2x). The combined organic layers were washed with brine, dried over $MgSO_4$, filtered and concentrated. The residue was purified by column chromatography (SiO_2; heptane/EtOAc 9:1) to obtain 513 g of **34** as a beige solid. Yield: 92 %. ^{1}H NMR (400 MHz, DMSO-d_6) δ 7.93 (dd, 1H), 7.62 (dd, 1H), 2.50 (s, 3H, overlapping with DMSO), 1.32 (s, 12H).

5-Fluoro-2-methyl-3-(4,4,5,5-tetramethyl-1,3,2-dioxaborolan-2-yl)aniline (35). To a solution of **34** (509 g, 1811 mmol) in MeOH (4.6 L) in an autoclave was added Pd-C 10 % (50 g). The mixture was evacuated and purged with hydrogen. The reaction mixture was stirred at RT under a hydrogen atmosphere for 7 h. The mixture was filtered through a suction filter and the filter cake was washed with MeOH. The filtrate was concentrated. The residue was purified by column chromatography (SiO_2; heptane/EtOAc gradient) to afford batch 1 (435 g) and batch 2 (5.4 g) of **35**. Batch 1 of **35** (435 g) was dissolved in hexane (1400 mL) under reflux and was allowed to cool to RT over 2 h while stirring. The precipitate was filtered off and washed with cold hexane, then dried in vacuo to afford 387 g of **35** as a white solid. The mother liquor was concentrated and combined with batch 2 of **35** (5.4 g). The residue was recrystallised from hexane (100 mL) as described above to afford 36 g of **35** as a white solid. The two batches were combined. Yield: 93 %. [ES-MS] (ESI+): m/z calcd for $C_{13}H_{20}BFNO_2$ $[M + H]^+$, 252.2; found, 252.2. ^{1}H NMR (400 MHz, DMSO-d_6) δ 6.52 – 6.45 (m, 2H), 5.09 (s, 2H), 2.17 (s, 3H), 1.28 (s, 12H).

Methyl 4-cyclopropyl-2-fluorobenzoate (**37**). A solution of methyl 4-bromo-2-fluorobenzoate (20.00 g, 84 mmol) and cyclopropylboronic acid (9.68 g, 109 mmol) in toluene was purged with argon for 5 min. Then, tricyclohexylphosphine (2.36 g, 8.41 mmol) and water (1.82 mL, 101

mmol) were added. The mixture was purged with argon for an additional 10 min. $Pd(OAc)_2$ (0.944 g, 4.21 mmol) was added and the reaction mixture was stirred at 100 °C overnight. The mixture was partitioned between EtOAc and water. The black suspension was filtered over a pad of Celite. The layers of the now clear mixture were separated. The aqueous layer was back-extracted with EtOAc. The combined organic layers were washed with saturated aqueous $NaHCO_3$ solution and brine, dried over $MgSO_4$, filtered and concentrated. The residue was purified by column chromatography (SiO_2; cyclohexane/EtOAc gradient) to obtain 17.00 g (purity 95 %) of **37** as a brown oil. Yield: 99 %. [ES-MS] (ESI+): m/z calcd for $C_{11}H_{12}FO_2$ $[M + H]^+$, 195.1; found, 195.1. ^1H NMR (400 MHz, DMSO-d_6) δ 7.79 – 7.69 (m, 1H), 7.04 (s, 1H), 7.03 – 6.99 (m, 1H), 3.81 (s, 3H), 2.06 – 1.95 (m, 1H), 1.10 – 1.00 (m, 2H), 0.85 – 0.73 (m, 2H).

4-Cyclopropyl-2-fluoro-N-(5-fluoro-2-methyl-3-(4,4,5,5-tetramethyl-1,3,2-dioxaborolan-2-yl)phenyl)benzamide (38). To a suspension of **35** (17.00 g, 64.3 mmol) and **37** (16.24 g, 84.0 mmol) in THF (300 mL) at 0 °C was added NaHMDS (1 M in THF, 96 mL, 96.0 mmol) dropwise. The reaction mixture was stirred at RT for 1 h, then more NaHMDS (1 M in THF, 20 mL, 20.0 mmol) was added. The reaction mixture was stirred at RT for 1 h. Then, a third batch of NaHMDS (1.0 M in THF, 20 mL, 20.0 mmol) was added and the reaction mixture was stirred at RT for another 2 h. The mixture was diluted with EtOAc and washed with saturated aqueous $NaHCO_3$ solution. The aqueous layer was back-extracted with EtOAc. The combined organic layers were washed with brine, dried over $MgSO_4$, filtered and concentrated. The residue was suspended in EtOAc and stirred at RT for 20 min. The solid was filtered off, washed with EtOAc and dried in vacuo to afford a first batch of **38** (17.8 g) as a beige solid. The filtrate was concentrated and the residue was suspended in EtOAc. The suspension was stirred at RT for 20 min. The resulting solid was filtered off, washed with EtOAc and dried in vacuo to afford a second batch of **38** (3.4 g) as a

beige solid. The two batches were combined. Yield: 76 %. [ES-MS] (ESI+): m/z calcd for $C_{23}H_{27}BF_2NO_3$ $[M + H]^+$, 414.2; found, 414.2. ^{1}H NMR (400 MHz, DMSO-d_6) δ 9.72 (d, *J* = 2.9 Hz, 1H), 7.67 – 7.59 (m, 1H), 7.52 (d, br, *J* = 9.9 Hz, 1H), 7.21 (dd, *J* = 8.7, 2.9 Hz, 1H), 7.10 – 7.03 (m, 2H), 2.38 (s, 3H), 2.08 – 1.97 (m, 1H), 1.32 (s, 12H), 1.10 – 1.01 (m, 2H), 0.83 – 0.75 (m, 2H).

6-Amino-4-chloro-5-methoxypyrimidine (40). To a solution of 4,6-dichloro-5-methoxypyrimidine (5.00 g, 27.9 mmol) in 2-propanol (40 mL) in an autoclave was added ammonium hydroxide (26 % in water, 5.0 mL, 33.5 mmol). The autoclave was sealed and the reaction mixture was stirred at 70 °C for 48 h. After cooling the mixture the precipitate was filtered off and washed with *n*-pentane and diethylether. The residue was dried in vacuo to obtain 4.40 g of **40** as a white solid. Yield: 94 %. [ES-MS] (ESI+): m/z calcd for $C_5H_7ClN_3O$ $[M + H]^+$, 160.0; found, 160.1. ^{1}H NMR (400 MHz, Chloroform-d) δ 8.12 (s, 1H), 5.29 (s, 2H), 3.89 (s, 3H).

6-Amino-4-chloro-5-pyrimidinol (41). To a solution of **40** (2.30 g, 13.69 mmol) in DCM (100 mL) at RT was slowly added boron tribromide (6.5 mL, 68.5 mmol) and the reaction mixture was stirred at 40 °C for 3 h. The mixture was quenched by slowly adding MeOH (50 mL) at -10 °C, stirred at RT for 12 h, then concentrated under reduced pressure. The residue was taken up in water and EtOAc. The mixture was basified with aqueous sodium carbonate solution (2 M) to pH 9-10. The aqueous layer was washed with EtOAc (discarded), acidified to pH 5-6 with aqueous HCl solution (5 M), then extracted with EtOAc (1x) and DCM (1x). The combined organic layers were washed with brine, dried over $MgSO_4$, filtered and concentrated to afford 1.30 g (purity 90 %) of **41** as a beige solid. Yield: 59 %. [ES-MS] (ESI+): m/z calcd for $C_4H_5ClN_3O$ $[M + H]^+$, 146.0; found, 146.0. ^{1}H NMR (400 MHz, DMSO-d_6) δ 9.57 (s, 1H), 7.78 (s, 1H), 6.89 (s, 2H).

***tert*-Butyl (2-((4-amino-6-chloropyrimidin-5-yl)oxy)ethyl)(methyl)carbamate (42).** To a solution of **41** (2.00 g, 13.7 mmol) in THF (120 mL) was added a solution of N-Boc-N-methyl-2-hydroxyethylamine (6.74 g, 38.5 mmol) in THF (5 mL) followed by Smopex-301 (1 mmol/g) (34.4 g, 34.4 mmol) and a solution of DIAD (6.68 mL, 34.4 mmol) in THF (15 mL). The reaction mixture was stirred at 60 °C for 2 h. The mixture was filtered through a pad of Celite. The filtrate was concentrated to afford a yellow oil. The residue was treated with EtOAc and sonicated to provide a suspension which was allowed to stand at RT for 1 h. The precipitate was filtered off and dried in vacuo to obtain 2.33 g (purity 95 %) of **42** as a white solid. Yield: 53 %. [ES-MS] (ESI+): m/z calcd for $C_{12}H_{20}ClN_4O_3$ $[M + H]^+$, 303.1; found, 303.0. ^{1}H NMR (400 MHz, DMSO-d_6) rotamers δ 7.97 (s, 1H), 7.27 (s, br, 2H), 4.04 – 3.89 (m, 2H), 3.59 – 3.48 (m, 2H), 2.97 – 2.81 (m, 3H), 1.47 – 1.30 (m, 9H).

***tert*-Butyl (2-((4-amino-6-(3-(4-cyclopropyl-2-fluorobenzamido)-5-fluoro-2-methyl-phenyl)pyrimidin-5-yl)oxy)ethyl)(methyl)carbamate (43).** The reaction was carried out using a Masterwave BTR microwave reactor with a 1000 mL vial. DME and water were purged with argon. To a solution of **42** (17.0 g, 56.2 mmol) and **38** (25.5 g, 61.8 mmol) in DME (264 mL) and water (38 mL) was added $PdCl_2(PPh_3)_2$ (1.971 g, 2.81 mmol) followed by aqueous Na_2CO_3 solution (1 M, 168 mL, 168 mmol). The reaction mixture was heated at 110 °C under microwave irradiation for 15 min. More **38** (1.4 g, 3.4 mmol) and $PdCl_2(PPh_3)_2$ (0.28 g, 0.40 mmol) were added. The reaction mixture was heated at 110 °C under microwave irradiation for an additional 10 min. The mixture was diluted with EtOAc (850 mL) and saturated aqueous $NaHCO_3$ solution (710 mL) and transferred into a separatory funnel. The layers were separated, the aqueous layer was back-extracted with EtOAc (425 mL). The combined organic layers were washed with brine, dried over Na_2SO_4, filtered and concentrated. The residue was triturated with EtOAc and the

mixture was stirred at RT for 30 min. The precipitate was filtered off and washed with EtOAc to afford 24.13 g (purity 97 %) of **43** as a light grey solid. Yield: 74 %. [ES-MS] (ESI+): m/z calcd for $C_{29}H_{34}F_2N_5O_4$ $[M + H]^+$, 554.3; found, 554.3. ^{1}H NMR (400 MHz, DMSO-d_6) rotamers δ 9.74 (s, br, 1H), 8.18 (s, 1H), 7.69 – 7.62 (m, 1H), 7.62 – 7.55 (m, 1H), 7.10 – 7.03 (m, 2H), 7.03 – 6.90 (m, 3H), 3.57 – 3.47 (m, 2H), 3.28 – 3.22 (m, 2H), 2.58 (s, 3H), 2.09 – 1.97 (m, 1H) overlapping with 2.04 (s, 3H), 1.33 and 1.29 (2s, br, total 9H), 1.10 – 1.01 (m, 2H), 0.84 – 0.75 (m, 2H).

Kinase Binding Assays

The kinase-binding assays in screening or K_d determination modes have been described[50,51] and were as follows: recombinant DNA-tagged kinase proteins were produced from kinase-tagged T7 phage strains or by producing the kinase protein in HEK-293 cells with subsequent tagging with DNA for qPCR detection. Streptavidin-coated magnetic beads were treated with biotinylated small molecule ligands for 30 minutes at room temperature to generate affinity resins for kinase assays. The liganded beads were blocked with excess biotin and washed with blocking buffer (SeaBlock (Pierce), 1% BSA, 0.05% Tween 20, 1 mM DTT) to remove unbound ligand and to reduce nonspecific binding. Binding reactions were assembled by combining kinases, liganded affinity beads, and test compounds in 1x binding buffer (20% SeaBlock, 0.17x PBS, 0.05% Tween 20, 6 mM DTT). Test compounds were prepared as 111X stocks in 100% DMSO. K_ds were determined using an 11-point 3-fold compound dilution series with three DMSO control points. All compounds for K_d measurements are distributed by acoustic transfer (non-contact dispensing) in 100% DMSO. The compounds were then diluted directly into the assays such that the final concentration of DMSO was 0.9%. All reactions were performed in polypropylene 384-well plates in a final volume of 0.02 ml. The assay plates were incubated at room temperature with shaking

for 1 hour and the affinity beads were washed with wash buffer (1x PBS, 0.05% Tween 20). The beads were then re-suspended in elution buffer (1x PBS, 0.05% Tween 20, 0.5 μM non-biotinylated affinity ligand) and incubated at room temperature with shaking for 30 minutes. The kinase concentration in the eluates was measured by qPCR.

Binding constants (K_d) were calculated with a standard dose-response curve using the Hill equation:

$$Response = Background + \frac{Signal - Background}{1 + (\frac{Kd^{Hill\ Slope}}{Dose^{Hill\ Slope}})}$$

The Hill Slope was set to -1 and curves were fitted using a non-linear least square fit with the Levenberg-Marquardt algorithm

BTK Occupancy

Covalent binding of compounds to BTK was determined with immunoassays for free BTK (i.e. not covalently occupied by compound) and total BTK protein. For free BTK measurements, samples were incubated with a biotinylated covalent BTK probe,[43] then samples were added to streptavidin ELISA plates to allow binding of probe-bound BTK. The binding of the probe to BTK is mutually exclusive with compound binding to BTK. Plate-bound BTK was detected with an anti-BTK antibody (D3H5, Cell Signaling Technology). For total BTK measurements, an ELISA plate was coated with D3H5 anti-BTK to capture total BTK. An anti-BTK antibody (#53, BD Biosciences) directed to a different epitope was then used to detect captured BTK. The respective free BTK levels for each sample were normalized to the total BTK level in the same sample and these ratios were expressed as percentage of the vehicle control samples.

Animal Studies

All animal studies described here were performed according to Swiss animal welfare laws and specifically according to animal licences BS-1182, BS-1151 and BS-1244 issued by the Basel-Stadt Cantonal Veterinary Office.

BTK Occupancy PK/PD model

To assess the PK/PD profile of the covalent BTK inhibitors, we measured BTK occupancy from tissue samples of animals treated with compounds. Female OFA-1 rats were dosed orally with compounds formulated at the indicated doses. Blood samples at 0.5, 2 and 5 hours after compound dosing were taken into EDTA tubes under deep anaesthesia for PK analysis. Five hours after dosing the animals were killed and the spleen removed to determine BTK target occupancy as described above (BTK occupancy assay).

ASSOCIATED CONTENT

Supporting Information

The supporting Information is available free of charge on the ACS Publication website at DOI:
Synthesis of compounds **9**-**24**, **26**-**32**; structural biology data; *in vitro* ADME profile of LOU064; biology data; animal studies; references (PDF)
Molecular formula strings (CSV)

Accession Codes

Authors will release the atomic coordinates and experimental data upon article publication. PDB ID accession codes 6S90, 6TFP.

AUTHOR INFORMATION

Corresponding Author

*E-mail: daniela.angst@novartis.com.

ACKNOWLEDGMENT

We thank G. Rosé, J. Karrer, E. Blum, E. Buccheri, O. Decoret, N. Fur, S. Ilic, M.-L. Manisse, B. Niepold, F. Ossola, G. Schwalm, S. Wildpreth, and D. Wiss for their synthetic support, P. Drueckes, D. Eichlisberger, S. Gaveriaux, and A.-S. Mangold for their efforts toward developing and performing biochemical and cellular assays, R. Keller, P. Ramseier and M. Vogelsanger for in *vivo* pharmacology, C. Marx and R. Denay for analytical data, and A. Lingel for GSH stability data. We are grateful to the MX beamline team at the Swiss Light Source (PSI Villigen, Switzerland) for outstanding support at the beamline and Expose GmbH (Switzerland) for diffraction data collection.

ABBREVIATIONS

ADME, absorption, distribution, metabolism, and excretion; BCR, B-cell receptor; BTK, Bruton's tyrosine kinase; CIA, collagen-induced arthritis; CL, clearance; CsA, cyclosporin; GSH, glutathione; IgM, immunoglobulin M; IL-4, interleukin-4; IL-8, interleukin-8; PAMPA, parallel artificial membrane permeability assay; PD, pharmacodynamic; PK, pharmacokinetic; SAR, structure-activity relationship; SRBC, sheep red blood cells; XLA, X-linked agammaglobulinemia.

REFERENCES

(1) Smith, C. I. E.; Islam, T. C.; Mattsson, P. T.; Mohamed, A. J.; Nore, B. F.; Vihinen, M. The Tec Family of Cytoplasmic Tyrosine Kinases: Mammalian Btk, Bmx, Itk, Tec, Txk and Homologs in Other Species. *BioEssays* **2001**, *23*, 436–446.

(2) Bradshaw, J. M. The Src, Syk, and Tec Family Kinases: Distinct Types of Molecular Switches. *Cell. Signal.* **2010**, *22*, 1175–1184.

(3) Satterthwaite, A. B.; Li, Z.; Witte, O. N. Btk Function in B Cell Development and Response. *Semin. Immunol.* **1998**, *10*, 309–316.

(4) Schmidt, U.; Boucheron, N.; Unger, B.; Ellmeier, W. The Role of Tec Family Kinases in Myeloid Cells. *Int. Arch. Allergy Immunol.* **2004**, *134*, 65–78.

(5) Brunner, C.; Müller, B.; Wirth, T. Bruton's Tyrosine Kinase Is Involved in Innate and Adaptive Immunity. *Histol. Histopathol.* **2005**, *20*, 945–955.

(6) Nyhoff, L. E.; Clark, E. S.; Barron, B. L.; Bonami, R. H.; Khan, W. N.; Kendall, P. L. Bruton's Tyrosine Kinase Is Not Essential for B Cell Survival beyond Early Developmental Stages. *J. Immunol.* **2018**, *200*, 2352–2361.

(7) Conley, M. E.; Dobbs, A. K.; Farmer, D. M.; Kilic, S.; Paris, K.; Grigoriadou, S.; Coustan-Smith, E.; Howard, V.; Campana, D. Primary B Cell Immunodeficiencies: Comparisons and Contrasts. *Annu. Rev. Immunol.* **2009**, *27*, 199–227.

(8) Khan, W. N.; Sideras, P.; Rosen, F. S.; Alt, F. W. The Role of Bruton's Tyrosine Kinase in B-Cell Development and Function in Mice and Man. *Ann. N. Y. Acad. Sci.* **1995**, *764*, 27–38.

(9) Howard, V.; Greene, J. M.; Pahwa, S.; Winkelstein, J. A.; Boyle, J. M.; Kocak, M.; Conley, M. E. The Health Status and Quality of Life of Adults with X-Linked Agammaglobulinemia. *Clin. Immunol.* **2006**, *118*, 201–208.

(10) Shillitoe, B.; Gennery, A. X-Linked Agammaglobulinaemia: Outcomes in the Modern Era. *Clin. Immunol.* **2017**, *183*, 54–62.

(11) Jansson, L.; Holmdahl, R. Genes on the X Chromosome Affect Development of Collagen-Induced Arthritis in Mice. *Clin. Exp. Immunol.* **1993**, *94*, 459–465.

(12) Steinberg, B. J.; Smathers, P. A.; Frederiksen, K.; Steinberg, A. D. Ability of the Xid Gene to Prevent Autoimmunity in (NZB X NZW)F1 Mice during the Course of Their Natural History, after Polyclonal Stimulation, or Following Immunization with DNA. *J. Clin. Invest.* **1982**, *70*, 587–597.

(13) Hata, D.; Kawakami, Y.; Inagaki, N.; Lantz, C. S.; Kitamura, T.; Khan, W. N.; Maeda-Yamamoto, M.; Miura, T.; Han, W.; Hartman, S. E.; Yao, L.; Nagai, H.; Goldfeld, A. E.; Alt, F. W.; Galli, S. J.; Witte, O. N.; Kawakami, T. Involvement of Bruton's Tyrosine Kinase in FcεRI-Dependent Mast Cell Degranulation and Cytokine Production. *J. Exp. Med.* **1998**, *187*, 1235–1247.

(14) Honigberg, L. A.; Smith, A. M.; Sirisawad, M.; Verner, E.; Loury, D.; Chang, B.; Li, S.; Pan, Z.; Thamm, D. H.; Miller, R. A.; Buggy, J. J. The Bruton Tyrosine Kinase Inhibitor PCI-32765 Blocks B-Cell Activation and Is Efficacious in Models of Autoimmune Disease and B-Cell Malignancy. *Proc. Natl. Acad. Sci.* **2010**, *107*, 13075–13080.

(15) Xu, D.; Kim, Y.; Postelnek, J.; Vu, M. D.; Hu, D.-Q.; Liao, C.; Bradshaw, M.; Hsu, J.;

Zhang, J.; Pashine, A.; Srinivasan, D.; Woods, J.; Levin, A.; O'Mahony, A.; Owens, T. D.; Lou, Y.; Hill, R. J.; Narula, S.; DeMartino, J.; Fine, J. S. RN486, a Selective Bruton's Tyrosine Kinase Inhibitor, Abrogates Immune Hypersensitivity Responses and Arthritis in Rodents. *J. Pharmacol. Exp. Ther.* **2012**, *341*, 90–103.

(16) Di Paolo, J. A.; Huang, T.; Balazs, M.; Barbosa, J.; Barck, K. H.; Bravo, B. J.; Carano, R. A. D. D.; Darrow, J.; Davies, D. R.; DeForge, L. E.; Diehl, L.; Ferrando, R.; Gallion, S. L.; Giannetti, A. M.; Gribling, P.; Hurez, V.; Hymowitz, S. G.; Jones, R.; Kropf, J. E.; Lee, W. P.; Maciejewski, P. M.; Mitchell, S. A.; Rong, H.; Staker, B. L.; Whitney, J. A.; Yeh, S.; Young, W. B.; Yu, C.; Zhang, J.; Reif, K.; Currie, K. S. Specific Btk Inhibition Suppresses B Cell– and Myeloid Cell–Mediated Arthritis. *Nat. Chem. Biol.* **2011**, *7*, 41–50.

(17) Rankin, A. L.; Seth, N.; Keegan, S.; Andreyeva, T.; Cook, T. a; Edmonds, J.; Mathialagan, N.; Benson, M. J.; Syed, J.; Zhan, Y.; Benoit, S. E.; Miyashiro, J. S.; Wood, N.; Mohan, S.; Peeva, E.; Ramaiah, S. K.; Messing, D.; Homer, B. L.; Dunussi-Joannopoulos, K.; Nickerson-Nutter, C. L.; Schnute, M. E.; Douhan 3rd, J.; Douhan 3rd, J. Selective Inhibition of BTK Prevents Murine Lupus and Antibody-Mediated Glomerulonephritis. *J Immunol* **2013**, *191*, 4540–4550.

(18) Watterson, S. H.; Liu, Q.; Beaudoin Bertrand, M.; Batt, D. G.; Li, L.; Pattoli, M. A.; Skala, S.; Cheng, L.; Obermeier, M. T.; Moore, R.; Yang, Z.; Vickery, R.; Elzinga, P. A.; Discenza, L. N.; D'Arienzo, C.; Gillooly, K. M.; Taylor, T. L.; Pulicicchio, C.; Zhang, Y.; Heimrich, E.; McIntyre, K. W.; Ruan, Q.; Westhouse, R. A.; Catlett, I. M.; Zheng, N.; Chaudhry, C.; Dai, J.; Galella, M. A.; Tebben, A. J.; Pokross, M.; Li, J.; Zhao, R.; Smith, D.; Rampulla, R. A.; Allentoff, A.; Wallace, M. A.; Mathur, A.; Salter-Cid, L.; Macor, J. E.; Carter, P. H.;

Fura, A.; Burke, J. R.; Tino, J. A.; Chen, L.; Obermeier, M. T.; Moore, R.; Yang, Z.; Vickery, R.; Elzinga, P. A.; Discenza, L. N.; D'Arienzo, C.; Gillooly, K. M.; Taylor, T. L.; Pulicicchio, C.; Zhang, Y.; Heimrich, E.; McIntyre, K. W.; Ruan, Q.; Westhouse, R. A.; Catlett, I. M.; Zheng, N.; Chaudhry, C.; Dai, J.; Galella, M. A.; Tebben, A. J.; Pokross, M.; Li, J.; Zhao, R.; Smith, D.; Rampulla, R. A.; Allentoff, A.; Wallace, M. A.; Mathur, A.; Salter-Cid, L.; Macor, J. E.; Carter, P. H.; Fura, A.; Burke, J. R.; Tino, J. A.; Cheng, L.; Obermeier, M. T.; Moore, R.; Yang, Z.; Vickery, R.; Elzinga, P. A.; Discenza, L. N.; D'Arienzo, C.; Gillooly, K. M.; Taylor, T. L.; Pulicicchio, C.; Zhang, Y.; Heimrich, E.; McIntyre, K. W.; Ruan, Q.; Westhouse, R. A.; Catlett, I. M.; Zheng, N.; Chaudhry, C.; Dai, J.; Galella, M. A.; Tebben, A. J.; Pokross, M.; Li, J.; Zhao, R.; Smith, D.; Rampulla, R. A.; Allentoff, A.; Wallace, M. A.; Mathur, A.; Salter-Cid, L.; Macor, J. E.; Carter, P. H.; Fura, A.; Burke, J. R.; Tino, J. A. Discovery of Branebrutinib (BMS-986195): A Strategy for Identifying a Highly Potent and Selective Covalent Inhibitor Providing Rapid in Vivo Inactivation of Bruton's Tyrosine Kinase (BTK). *J. Med. Chem.* **2019**, *62*, 3228–3250.

(19) Watterson, S. H.; De Lucca, G. V.; Shi, Q.; Langevine, C. M.; Liu, Q.; Batt, D. G.; Beaudoin Bertrand, M.; Gong, H.; Dai, J.; Yip, S.; Li, P.; Sun, D.; Wu, D.-R.; Wang, C.; Zhang, Y.; Traeger, S. C.; Pattoli, M. A.; Skala, S.; Cheng, L.; Obermeier, M. T.; Vickery, R.; Discenza, L. N.; D'Arienzo, C. J.; Zhang, Y.; Heimrich, E.; Gillooly, K. M.; Taylor, T. L.; Pulicicchio, C.; McIntyre, K. W.; Galella, M. A.; Tebben, A. J.; Muckelbauer, J. K.; Chang, C.; Rampulla, R.; Mathur, A.; Salter-Cid, L.; Barrish, J. C.; Carter, P. H.; Fura, A.; Burke, J. R.; Tino, J. A. Discovery of 6-Fluoro-5-(R)-(3-(S)-(8-Fluoro-1-Methyl-2,4-Dioxo-1,2-Dihydroquinazolin-3(4H)-Yl)-2-Methylphenyl)-2-(S)-(2-Hydroxypropan-2-Yl)-2,3,4,9-Tetrahydro-1H-Carbazole-8-Carboxamide (BMS-986142): A Reversible Inhibitor of

Bruton's Tyrosine (BTK) Conformationally Constrained by Two Locked Atropisomers. *J. Med. Chem.* **2016**, *59*, 9173–9200.

(20) Gillooly, K. M.; Pulicicchio, C.; Pattoli, M. A.; Cheng, L.; Skala, S.; Heimrich, E. M.; McIntyre, K. W.; Taylor, T. L.; Kukral, D. W.; Dudhgaonkar, S.; Nagar, J.; Banas, D.; Watterson, S. H.; Tino, J. A.; Fura, A.; Burke, J. R. Bruton's Tyrosine Kinase Inhibitor BMS-986142 in Experimental Models of Rheumatoid Arthritis Enhances Efficacy of Agents Representing Clinical Standard-of-Care. *PLoS One* **2017**, *12*, e0181782.

(21) Crawford, J. J.; Johnson, A. R.; Misner, D. L.; Belmont, L. D.; Castanedo, G.; Choy, R.; Coraggio, M.; Dong, L.; Eigenbrot, C.; Erickson, R.; Ghilardi, N.; Hau, J.; Katewa, A.; Kohli, P. B.; Lee, W.; Lubach, J. W.; McKenzie, B. S.; Ortwine, D. F.; Schutt, L.; Tay, S.; Wei, B.; Reif, K.; Liu, L.; Wong, H.; Young, W. B. Discovery of GDC-0853: A Potent, Selective, and Noncovalent Bruton's Tyrosine Kinase Inhibitor in Early Clinical Development. *J. Med. Chem.* **2018**, *61*, 2227–2245.

(22) Haselmayer, P.; Camps, M.; Liu-Bujalski, L.; Nguyen, N.; Morandi, F.; Head, J.; O'Mahony, A.; Zimmerli, S. C.; Bruns, L.; Bender, A. T.; Schroeder, P.; Grenningloh, R. Efficacy and Pharmacodynamic Modeling of the BTK Inhibitor Evobrutinib in Autoimmune Disease Models. *J. Immunol.* **2019**, *202*, 2888–2906.

(23) Singh, J.; Petter, R. C.; Kluge, A. F. Targeted Covalent Drugs of the Kinase Family. *Curr. Opin. Chem. Biol.* **2010**, *14*, 475–480.

(24) Barf, T.; Kaptein, A. Irreversible Protein Kinase Inhibitors: Balancing the Benefits and Risks. *J. Med. Chem.* **2012**, *55*, 6243–6262.

(25) Singh, J.; Petter, R. C.; Baillie, T. A.; Whitty, A. The Resurgence of Covalent Drugs. *Nat. Rev. Drug Discov.* **2011**, *10*, 307–317.

(26) Kalgutkar, A. S.; Dalvie, D. K. Drug Discovery for a New Generation of Covalent Drugs. *Expert Opin. Drug Discov.* **2012**, *7*, 561–581.

(27) Norman, P. Investigational Bruton's Tyrosine Kinase Inhibitors for the Treatment of Rheumatoid Arthritis. *Expert Opin. Investig. Drugs* **2016**, *25*, 891–899.

(28) Lanning, B. R.; Whitby, L. R.; Dix, M. M.; Douhan, J.; Gilbert, A. M.; Hett, E. C.; Johnson, T. O.; Joslyn, C.; Kath, J. C.; Niessen, S.; Roberts, L. R.; Schnute, M. E.; Wang, C.; Hulce, J. J.; Wei, B.; Whiteley, L. O.; Hayward, M. M.; Cravatt, B. F. A Road Map to Evaluate the Proteome-Wide Selectivity of Covalent Kinase Inhibitors. *Nat. Chem. Biol.* **2014**, *10*, 760–767.

(29) Médard, G.; Pachl, F.; Ruprecht, B.; Klaeger, S.; Heinzlmeir, S.; Helm, D.; Qiao, H.; Ku, X.; Wilhelm, M.; Kuehne, T.; Wu, Z.; Dittmann, A.; Hopf, C.; Kramer, K.; Kuster, B. Optimized Chemical Proteomics Assay for Kinase Inhibitor Profiling. *J. Proteome Res.* **2015**, *14*, 1574–1586.

(30) Molica, S. The Clinical Safety of Ibrutinib in Chronic Lymphocytic Leukemia. *Expert Opin. Drug Saf.* **2015**, *14*, 1621–1629.

(31) Shatzel, J. J.; Olson, S. R.; Tao, D. L.; McCarty, O. J. T.; Danilov, A. V.; DeLoughery, T. G. Ibrutinib-Associated Bleeding: Pathogenesis, Management, and Risk Reduction Strategies. *J. Thromb. Haemost.* **2017**, *38*, 1–13.

(32) Byrd, J. C.; Furman, R. R.; Coutre, S. E.; Burger, J. a; Blum, K. a; Coleman, M.; Wierda,

W. G.; Jones, J. a; Zhao, W.; Heerema, N. a; Johnson, A. J.; Shaw, Y.; Bilotti, E.; Zhou, C.; James, D. F.; O'Brien, S. Three-Year Follow-up of Treatment-Naive and Previously Treated Patients with CLL and SLL Receiving Single-Agent Ibrutinib. *Blood* **2015**, *125*, 2497–2506.

(33) Wang, M. L.; Blum, K. a; Martin, P.; Goy, A.; Auer, R.; Kahl, B. S.; Jurczak, W.; Advani, R. H.; Romaguera, J. E.; Williams, M. E.; Barrientos, J. C.; Chmielowska, E.; Radford, J.; Stilgenbauer, S.; Dreyling, M.; Jedrzejczak, W. W.; Johnson, P.; Spurgeon, S. E.; Zhang, L.; Baher, L.; Cheng, M.; Lee, D.; Beaupre, D. M.; Rule, S. Long-Term Follow-up of MCL Patients Treated with Single-Agent Ibrutinib: Updated Safety and Efficacy Results. *Blood* **2015**, *126*, 739–745.

(34) Leong, D. P.; Caron, F.; Hillis, C.; Duan, A.; Healey, J. S.; Fraser, G.; Siegal, D. The Risk of Atrial Fibrillation with Ibrutinib Use: A Systematic Review and Meta-Analysis. *Blood* **2016**, *128*, 138–140.

(35) Lucchini, E.; Pilotto, S.; Spada, E.; Melisi, D.; Bria, E.; Tortora, G. Targeting the Epidermal Growth Factor Receptor in Solid Tumors: Focus on Safety. *Expert Opin. Drug Saf.* **2014**, *13*, 535–549.

(36) Quek, L. S.; Bolen, J.; Watson, S. P. A Role for Bruton's Tyrosine Kinase (Btk) in Platelet Activation by Collagen. *Curr. Biol.* **1998**, *8*, 1137–1140.

(37) Nicolson, P. L. R.; Hughes, C. E.; Watson, S.; Nock, S. H.; Hardy, A. T.; Watson, C. N.; Montague, S. J.; Clifford, H.; Huissoon, A. P.; Malcor, J.-D.; Thomas, M. R.; Pollitt, A. Y.; Tomlinson, M. G.; Pratt, G.; Watson, S. P. Inhibition of Btk by Btk-Specific Concentrations of Ibrutinib and Acalabrutinib Delays but Does Not Block Platelet Aggregation Mediated

by Glycoprotein VI. *Haematologica* **2018**, *103*, 2097–2108.

(38) Barf, T.; Covey, T.; Izumi, R.; van de Kar, B.; Gulrajani, M.; van Lith, B.; van Hoek, M.; de Zwart, E.; Mittag, D.; Demont, D.; Verkaik, S.; Krantz, F.; Pearson, P. G.; Ulrich, R.; Kaptein, A. Acalabrutinib (ACP-196): A Covalent Bruton Tyrosine Kinase Inhibitor with a Differentiated Selectivity and In Vivo Potency Profile. *J. Pharmacol. Exp. Ther.* **2017**, *363*, 240–252.

(39) Chen, J.; Kinoshita, T.; Gururaja, T.; Sukbuntherng, J.; James, D.; Lu, D.; Whang, J.; Versele, M.; Chang, B. Y. The Effect of Bruton's Tyrosine Kinase (BTK) Inhibitors on Collagen-Induced Platelet Aggregation, BTK, and Tyrosine Kinase Expressed in Hepatocellular Carcinoma (TEC). *Eur. J. Haematol.* **2018**, *101*, 604–612.

(40) Dittus, L.; Werner, T.; Muelbaier, M.; Bantscheff, M. Differential Kinobeads Profiling for Target Identification of Irreversible Kinase Inhibitors. *ACS Chem. Biol.* **2017**, *12*, 2515–2521.

(41) Young, W. B.; Barbosa, J.; Blomgren, P.; Bremer, M. C.; Crawford, J. J.; Dambach, D.; Gallion, S.; Hymowitz, S.; Kropf, J. E.; Lee, S. H.; Liu, L.; Lubach, J.; Macaluso, J.; Maciejewski, P.; Maurer, B.; Mitchell, S. a.; Ortwine, D. F.; Paolo, J. Di; Reif, K.; Scheerens, H.; Schmitt, A.; Gregory Sowell, C.; Wang, X.; Wong, H.; Xiong, J.-M.; Xu, J.; Zhao, Z.; Currie, K. S. Potent and Selective Bruton's Tyrosine Kinase Inhibitors: Discovery of GDC-0834. *Bioorg. Med. Chem. Lett.* **2015**, 1–5.

(42) Bender, A. T.; Gardberg, A.; Pereira, A.; Johnson, T.; Wu, Y.; Grenningloh, R.; Head, J.; Morandi, F.; Haselmayer, P.; Liu-Bujalski, L. Ability of Bruton's Tyrosine Kinase Inhibitors to Sequester Y551 and Prevent Phosphorylation Determines Potency for

Inhibition of Fc Receptor but Not B-Cell Receptor Signaling. *Mol. Pharmacol.* **2017**, *91*, 208–219.

(43) Pulz, R.; Angst, D.; Dawson, J.; Gessier, F.; Gutmann, S.; Hersperger, R.; Hinniger, A.; Janser, P.; Koch, G.; Revesz, L.; Vulpetti, A.; Waelchli, R.; Zimmerlin, A.; Cenni, B. Design of Potent and Selective Covalent Inhibitors of Bruton's Tyrosine Kinase Targeting an Inactive Conformation. *ACS Med. Chem. Lett.* **2019**, *10*, 1467–1472.

(44) Liang, Q.; Chen, Y.; Yu, K.; Chen, C.; Zhang, S.; Wang, A.; Wang, W.; Wu, H.; Liu, X.; Wang, B.; Wang, L.; Hu, Z.; Wang, W.; Ren, T.; Zhang, S.; Liu, Q.; Yun, C.-H.; Liu, J. Discovery of N-(3-(5-((3-Acrylamido-4-(Morpholine-4-Carbonyl)Phenyl)Amino)-1-Methyl-6-Oxo-1,6-Dihydropyridin-3-Yl)-2-Methylphenyl)-4-(Tert-Butyl)Benzamide (CHMFL-BTK-01) as a Highly Selective Irreversible Bruton's Tyrosine Kinase (BTK) Inhibitor. *Eur. J. Med. Chem.* **2017**, *131*, 107–125.

(45) Zhao, Z.; Bourne, P. E. Progress with Covalent Small-Molecule Kinase Inhibitors. *Drug Discov. Today* **2018**, *23*, 727–735.

(46) Dalvit, C.; Vulpetti, A. Intermolecular and Intramolecular Hydrogen Bonds Involving Fluorine Atoms: Implications for Recognition, Selectivity, and Chemical Properties. *ChemMedChem* **2012**, *7*, 262–272.

(47) Palkowitz, M. D.; Tan, B.; Hu, H.; Roth, K.; Bauer, R. A. Synthesis of Diverse N -Acryloyl Azetidines and Evaluation of Their Enhanced Thiol Reactivities. *Org. Lett.* **2017**, *19*, 2270–2273.

(48) Copeland, R. A. Evaluation of Enzyme Inhibitors in Drug Discovery. A Guide for Medicinal

Chemists and Pharmacologists. *Methods Biochem. Anal.* **2005**, *46*, 1–265.

(49) Paulini, R.; Müller, K.; Diederich, F. Orthogonal Multipolar Interactions in Structural Chemistry and Biology. *Angew. Chemie Int. Ed.* **2005**, *44*, 1788–1805.

(50) Fabian, M. A.; Biggs, W. H.; Treiber, D. K.; Atteridge, C. E.; Azimioara, M. D.; Benedetti, M. G.; Carter, T. A.; Ciceri, P.; Edeen, P. T.; Floyd, M.; Ford, J. M.; Galvin, M.; Gerlach, J. L.; Grotzfeld, R. M.; Herrgard, S.; Insko, D. E.; Insko, M. a; Lai, A. G.; Lélias, J.-M.; Mehta, S. a; Milanov, Z. V; Velasco, A. M.; Wodicka, L. M.; Patel, H. K.; Zarrinkar, P. P.; Lockhart, D. J. A Small Molecule–Kinase Interaction Map for Clinical Kinase Inhibitors. *Nat. Biotechnol.* **2005**, *23*, 329–336.

(51) Wodicka, L. M.; Ciceri, P.; Davis, M. I.; Hunt, J. P.; Floyd, M.; Salerno, S.; Hua, X. H.; Ford, J. M.; Armstrong, R. C.; Zarrinkar, P. P.; Treiber, D. K. Activation State-Dependent Binding of Small Molecule Kinase Inhibitors: Structural Insights from Biochemistry. *Chem. Biol.* **2010**, *17*, 1241–1249.

(52) Berg, E. L.; Yang, J.; Melrose, J.; Nguyen, D.; Privat, S.; Rosler, E.; Kunkel, E. J.; Ekins, S. Chemical Target and Pathway Toxicity Mechanisms Defined in Primary Human Cell Systems. *J. Pharmacol. Toxicol. Methods* **2010**, *61*, 3–15.

(53) Copeland, R. A.; Pompliano, D. L.; Meek, T. D. Drug-Target Residence Time and Its Implications for Lead Optimization. *Nat. Rev. Drug Discov.* **2006**, *5*, 730–739.

(54) Evans, E. K.; Tester, R.; Aslanian, S.; Karp, R.; Sheets, M.; Labenski, M. T.; Witowski, S. R.; Lounsbury, H.; Chaturvedi, P.; Mazdiyasni, H.; Zhu, Z.; Nacht, M.; Freed, M. I.; Petter, R. C.; Dubrovskiy, A.; Singh, J.; Westlin, W. F. Inhibition of Btk with CC-292 Provides

Early Pharmacodynamic Assessment of Activity in Mice and Humans. *J. Pharmacol. Exp. Ther.* **2013**, *346*, 219–228.

(55) Jerne, N. K.; Nordin, A. A. Plaque Formation in Agar by Single Antibody-Producing Cells. *Science.* **1963**, *140*, 405.

(56) Trentham, D. E.; Townes, A. S.; Kang, A. H. Autoimmunity to Type II Collagen an Experimental Model of Arthritis. *J. Exp. Med.* **1977**, *146*, 857–868.

(57) Durie, F. H.; Fava, R. A.; Noelle, R. J. Collagen-Induced Arthritis as a Model of Rheumatoid Arthritis. *Clin. Immunol. Immunopathol.* **1994**, *73*, 11–18.

(58) Williams, R. O. Collagen-Induced Arthritis in Mice: A Major Role for Tumor Necrosis Factor-α. In *Target Discovery and Validation Reviews and Protocols*; Humana Press: New Jersey, 2007; Vol. 361, pp 265–284.

(59) Kaul, M.; Storim, J.; End, P.; Cabanski, M.; Jakab, A.; Schuhler, C.; Funhoff, E.; Schaefer, F.; Dimanova, E.; Kistowska, M.; Kinhikar, A.; Maiolica, A.; Sinn, A.; Fuhr, R.; Cenni, B. Abstracts from the European Academy of Allergy and Clinical Immunology Congress, 01–05 June 2019, Lisbon, Portugal. *Allergy* **2019**, *74*, 332.

For Table of Contents Only

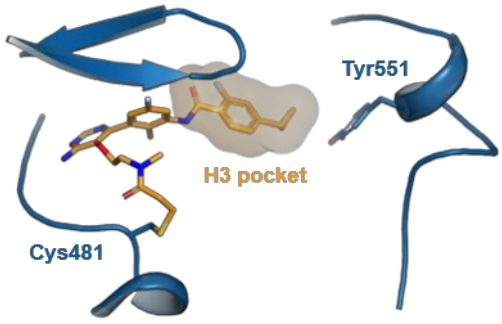
Tyr551
H3 pocket
Cys481